AALBORG UNIVERSITY
STUDENT REPORT

Mathematically modeling the electrical activity of a wedge of left ventricular heart tissue.

4. Semester – Master Thesis – Spring 2019

Group 19gr10413

AALBORG UNIVERSITY
STUDENT REPORT

4th Semester, Master Thesis

School of Medicine and Health

Biomedical Engineering and Informatics

Frederik Bajers Vej 7A, 9220 Aalborg

Title:
Mathematically modeling the electrical activity of a wedge of left ventricular heart tissue.

Project period:
Spring 2019
01/02/2019 – 06/06/2019

Project group:
19gr10413

Participant:
Annabel Christin Bantle

Supervisors:
Johannes Jan Struijk
Jacob Klit Seidelin Melgaard

Pages:
40

Handed in:
06/06/2019

Synopsis

Electrocardiography is a widely used diagnostic method to detect abnormalities in the electrical activity of the heart. Although ECGs have been used for many years, the emergence of the T wave and details of associated physiological processes have been a matter of controversy for decades. The T wave genesis has been investigated with an array of experimental heart models. Particularly the wedge preparations from canine hearts showed findings contrary to classical assumptions. It is of interest to know, whether findings from the wedge preparation are concordant with physiological electrical behavior of ventricular heart tissue.

Since the internal processes within the wedge are not accessible, mathematical modelling is used to access the underlying processes of the wedge preparation. The increase in computational power facilitates the use of more detailed mathematical models.

The aim of this project was to develop and implement a mathematical bidomain model of a wedge of human left ventricular heart tissue and therewith reconstructing mathematically the setup of a wedge preparation for human tissue.

Content

1 Introduction 3
2 Background 4
2.1 Electrical activity of the heart 4
2.1.1 Conduction system of the heart 4
2.1.2 Cardiac action potential 5
2.1.3 Electrocardiogram 6
2.1.4 Controversy of the T wave 7
2.2 Modeling heart tissue 8
2.3 Wedge model 9
3 Objective 10
4 Methods 11
4.1 Bidomain model 11
4.1.1 Mathematical formulation of the bidomain model 12
4.1.2 Boundary conditions 13
4.1.3 Solving bidomain equations 14
4.2 Ionic current model 15
4.3 Simulating the electrical activity of wedge of heart tissue 17
5 Results 18
5.1 Bidomain model 18
5.2 Simulating the electrical activity of wedge of heart tissue 20
6 Discussion 24
6.1 Bidomain model 24
6.2 Simulating the electrical activity of wedge of heart tissue 24
7 Conclusion 25
References 26
Appendix A 30
Appendix B 36

1 Introduction

Electrocardiography is a widely used and valuable diagnostic method to detect abnormalities in the electrical activity of the heart [1–4]. Even though electrocardiograms (ECGs) have been indispensable for about a century, the exact genesis of all its waveforms is hitherto not completely determined. In particular, the emergence of the T wave has been a matter of controversy for decades. [3,4]
Electrophysiological backgrounds of the T wave genesis have been investigated in human cardiac tissue and animal models. These models range from full heart models to wedge preparations of cardiac tissue. [3–6] Especially wedge preparations from canine hearts showed findings contrary to the classical ideas [3,5,7–10].
However, often it is complicated or simply not possible to study ongoing processes under physiological conditions in a 3D manner [11]. Besides, animal models may differ from human physiology [12,13]. To overcome those limitations, mathematical modelling can be used [11–13].
Mathematical models are mostly computer-based models, hence the increase in computational power facilitates the use of computationally heavy detailed mathematical models. [1,14] Computer-based models have gained popularity in investigating physiological processes ongoing in cardiac tissue, and allow to deepen and broaden knowledge in electrophysiology [15–17]. It is possible to simulate various conditions with models in order to reconstruct experiments and compare the findings [14].

Since the electrical activity of the heart emerges from complex interrelations of microscopic factors, such as ion exchange, and macroscopic factors, such as anisotropic behaviour, a challenge in mathematical modelling is to affiliate different anatomical and physiological compartments of particular levels [14,16]. Therefore it is often required to interlink various models [14].
The numerical simulation of cardiac electrical activity with the bidomain model is a valid tool for investigation of cardiac tissue [18,19]. The bidomain model is commonly used and well suited to simulate electrical activity of the heart on account of its integrity. Moreover it has been validated with animal experiments [20].

The aim of this project was to develop and implement a mathematical bidomain model of a wedge of human left ventricular heart tissue and therewith reconstruct mathematically the setup of a wedge preparation for human tissue.

2 Background

2.1 Electrical activity of the heart

2.1.1 Conduction system of the heart

The heart is autorhythmic and therefore initiates contractions with specialized muscle cells, so called pacemaker cells [1,21]. Figure 1 illustrates a cross section of a heart, with the conduction system is highlighted in green.

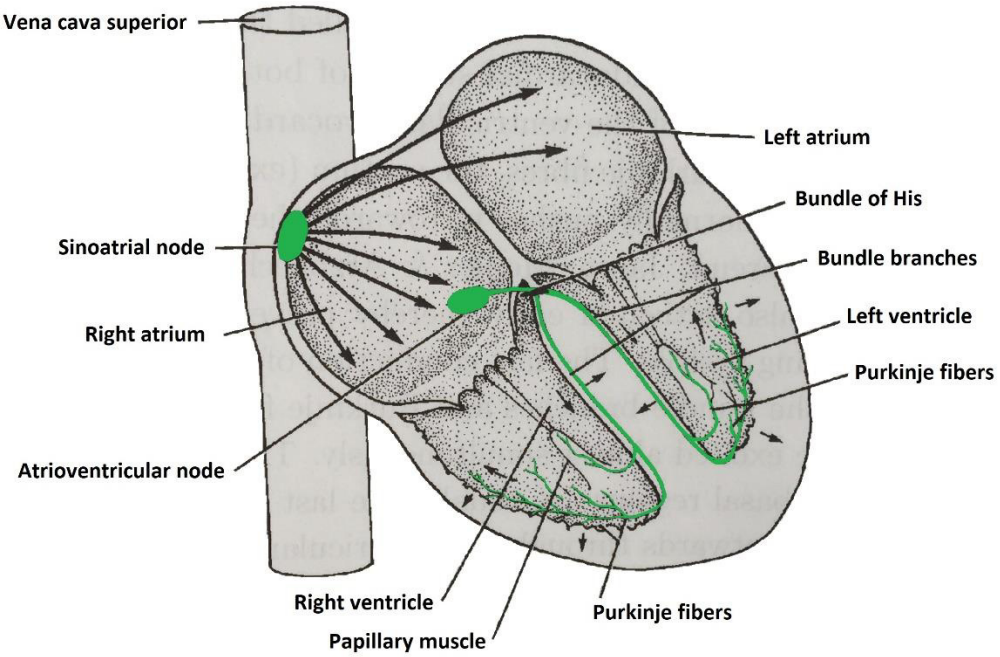

Figure 1: Schematic cross section of a heart. The conduction system is highlighted in green. Black arrows indicate propagation of depolarization. (Modified [1].)

The primary element of the conduction system is the sinoatrial node, which is located in the right atrium near the inlet of the vena cava superior. The sinoatrial node generates periodic stimuli in form of action potentials. This periodic stimulation, so called sinus rhythm, triggers depolarization, which proceeds through the right atrium into the left atrium and until the atrioventricular node. The atrioventricular node is located between the atria and the ventricles and is the only electrical connection of atria and ventricles. Thence the atrioventricular node is conducting the electrical activity to the bundle of His. [1,21] Moreover the conduction velocity is slowed down by the atrioventricular node to give the atria necessary time to contract [1].

The bundle of His divides into left and right bundle branches, running down the left and right septum wall respectively. The left bundle branch is passing through the membrane and dividing further into anterior and posterior branches. Close to the apex the bundle branches divide further into a network of Purkinje fibers, which spread across the surface of the endocardium and into the midmyocardium and pass the electrical activity on to the ventricular tissue. [1,21] Irrespective of the base, the septum is depolarized first [1]. Rapid conduction via the bundle branches and the Purkinje fibers enables almost simultaneous depolarization of the endocardium. The depolarization proceeds through the

ventricular walls outwardly. [1,21] Cell-to-cell activation propagates depolarization through ventricular tissue [21].
After depolarization repolarization comes to pass. Thereby no propagation occurs since the repolarization depends on the action potential duration of each cell and, contrary to depolarization, cannot be caused by neighbor cells. Since action potentials are shorter in the epicardium than in the endocardium, repolarization proceeds opposite to depolarization. [21]

2.1.2 Cardiac action potential

Each cardiac cell is surrounded by a cell membrane, which consists of a phospholipid bilayer. Inside the cell membrane is referred to as intracellular space and outside the cell membrane as extracellular space. In the phospholipid bilayer structure of the cell membrane proteins are integrated. These proteins function as ion channels for certain ions under particular conditions, resulting in selective permeability of the membrane. The selective permeability together with ion pumps lead to concentration gradients of ions and allows a potential difference across the membrane, i.e. between intracellular and extracellular space. Thereby the ions of major interest are K^+, Na^+ and Ca^{2+}. [1,2]

There are two forces regulating the ion flow and therewith the potential difference across the membrane. The chemical force is the concentration gradient, which leads to movement of ions and thus movement of electrical charge. This provokes an electrical gradient converse to the chemical gradient. An equilibrium between those two forces on one type of ion describes the Nernst potential. [1,2]

The potential difference across the membrane is the transmembrane potential or membrane potential. In a resting state the membrane potential is around -86 mV, more or less the Nernst potential of K^+. If a sufficing stimulus is applied and the membrane potential exceeds the threshold potential, an action potential is provoked. [1,2] An action potential is shown in Figure 2.

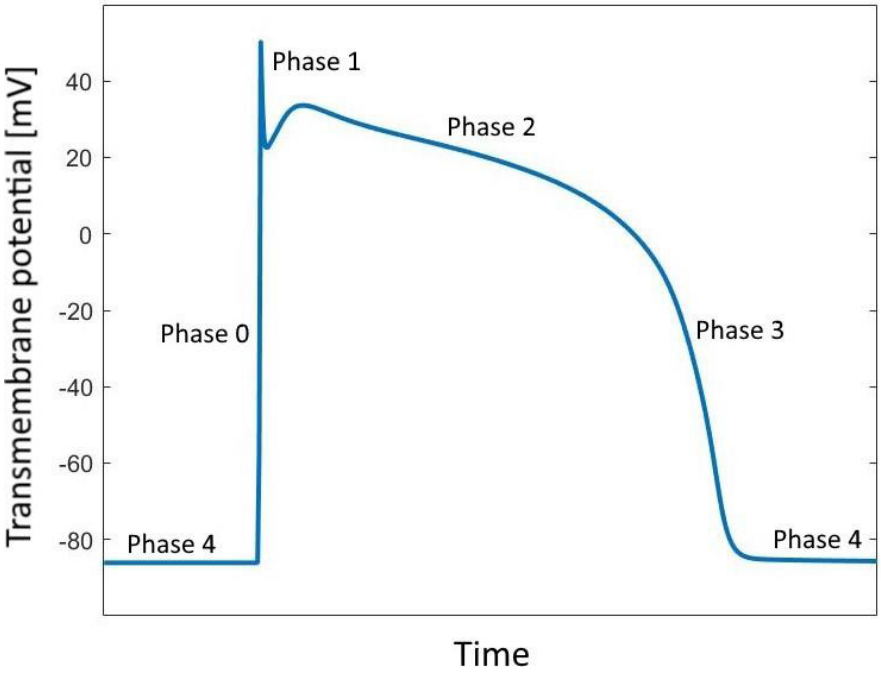

Figure 2: Action potential of cardiac cell.

During an action potential depolarization is caused by rapid influx of Na^+ into the intracellular space via fast opening Na^+ channels (Phase 0). This is followed by efflux of K^+ resulting in repolarization (Phase 1) until Ca^{2+} influx, balancing K^+ efflux resulting in a plateau phase (Phase 2). After termination of Ca2+ influx, persisting K^+ efflux continues repolarization (Phase 3) until the resting potential is reached again (Phase 4). [1,2]

The changes in the membrane potential due to current flow can be replicated by an equivalent electric circuit. Thereby the cell membrane is depicted by a capacitance in parallel with a set of resistors depicting ion channels incorporated in the membrane. [1] An example for this is illustrated in Figure 3.

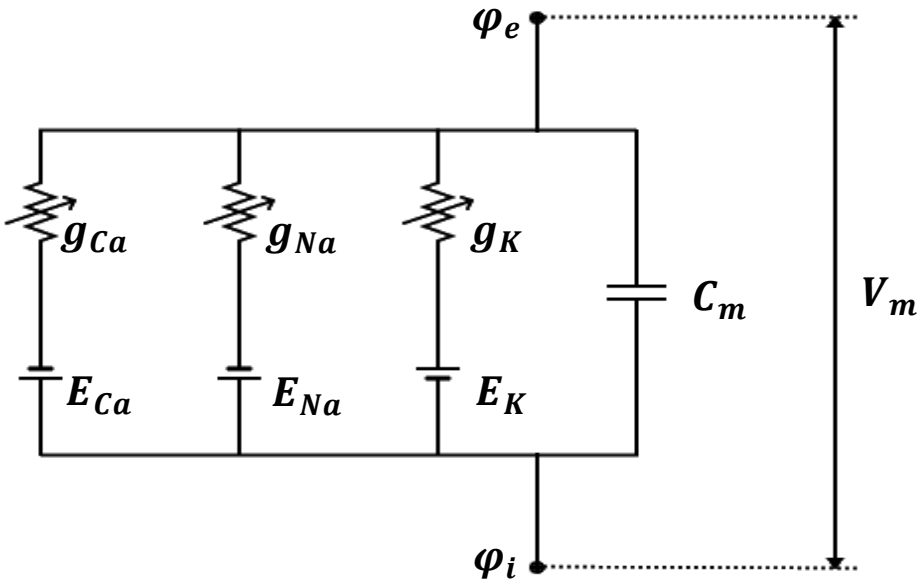

Figure 3: Electrical circuit representing the changes in membrane potential of the Hodgkin-Huxley model.

Thereby the ionic current through the membrane is represented by the capacitance C_m and the ion channels in parallel. The ion flow through a specific channel is given by its conductance g. This electrical circuit is describing the basic Hodgkin-Huxley model. [1] A more specific model is described in section 4.2.

2.1.3 Electrocardiogram

August Desiré Waller pioneered electrocardiography in 1887 by placing his dog's legs in buckets filled with saline solutions, which functioned as electrodes, and recorded the electrical activity of his dog's heart [1]. A similar experiment was conducted on humans. Whereby the voltage difference between two electrodes was recorded as a function of time on the body surface with a capillary electrometer [1,2]. Therewith the electrocardiogram (ECG), a recording of the electrical activity of the heart, was introduced. Einthoven, who witnessed Waller's experiment and ECG recording, developed the method further [1]. He invented the string galvanometer, which was used for the first commercially available ECG recorders and qualitatively even comparable to contemporary devices. Einthoven wanted to ensure a uniform nomenclature when referring to the deflections of ECGs and named the waves of the ECG recording P,Q,R,S and T. [1,2]

The electrical activity of the heart can be measured on the body surface, since it propagates passively through the surrounding tissue in the body [1,2,21]. Hence an ECG is a non-invasive tool to measure and visualize the cardiac electrical function, which makes it a powerful diagnostic tool [1,2].
The ECG displays the depolarization and repolarization of all cardiac cells superimposed. Hence the ECG shows the general electrical activity of the atria and the ventricles. [1] A normal ECG waveform is illustrated in Figure 4.

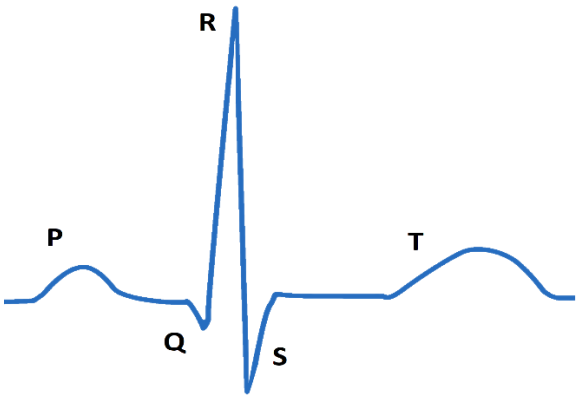

Figure 4: Normal waveform of an ECG signal. (Modified [22] .)

In an ECG the P wave depicts the depolarisation of the atria, and the QRS complex the depolarization of the ventricles [1,2]. The P wave demonstrates, compared to the QRS complex, lower magnitude since less cells are activated [2].

The T wave depicts the ventricular repolarization. The atrial repolarization is not visible in the ECG since it occurs simultaneously with the QRS complex, which is overlaying the atrial repolarization due to its greater magnitude. [1,2,21]

2.1.4 Controversy of the T wave

Although the ECG has been a valuable tool to measure the electrical activity of the heart for over a century by now, the exact genesis of all waveforms is not completely understood yet. Especially the emergence of the T wave has been vigorously contested for years. [3,4]
General agreement is that the T wave is caused by ventricular repolarization [1–6,23,24]. Early studies and contemporary textbooks support the hypothesis that depolarization and repolarization proceed in opposite directions. Those studies found that repolarization occurs earlier at base compared to apex, wherefore an apico-basal gradient in repolarization has been assumed. [2,5,6,23,24]
However Patel et al. [3] criticize this assumption by claiming that the measurement of epicardial cells at the apex and endocardial cells at the base represent a transmural gradient in repolarization instead.

In the 1970s a transmural gradient in repolarization was introduced by several studies [3,25]. Supporting this, Franz et al. [26] found that the duration of repolarization is shorter in the epicardium than in the endocardium as well as earlier repolarization of later activated areas and conclude the presence of a predominant transmural gradient in repolarization.
In the 1990s so called M cells were discovered and were claimed to cause a transmural gradient in repolarization due to increased action potential duration compared to epicardium and endocardium

[3,27]. However there is disagreement whether M cells exist, since they were observed in wedge models but not in vivo. Furthermore it is assumed that human hearts do not comprise M cells. [4]
In the late 2000s Patel et al. [3] found in a wedge model preparation (see section 2.3) a significant difference in the action potential durations of endocardium and epicardium. A significant difference in the action potential duration of the apex and the base was not found [3]. Therewith Patel et al. [3] underline the presence of a transmural repolarization gradient causing the morphology of the T wave and conclude that the transmural gradient in repolarization is caused by the difference in action potential duration of endocardium and epicardium. The presence of an apico-basal gradient is not precluded, though considered as neglectable. On the grounds of a greater distance for the apico-basal gradient than for the transmural gradient it is explained that the transmural gradient in repolarization is of greater influence since the effect of the gradient depends on its steepness. [3]
Whereas Moore et al. [28] stated already in 1965 that it was not possible to conclude that the differences in the action potential duration of endocardium and epicardium are causing the T wave morphology.

Meijborg et al. [4] investigated gradients in repolarization along anatomical axes and found significant apico-basal and transmural gradients in repolarization. Nevertheless none of the gradients was intense enough to cause the T wave morphology singlehandedly, hence the gradients along all anatomical axes contribute [4].
On the same token, Opthof et al. [5] compared the percentage proportion of different gradients in repolarization. The results show that a transmural gradient in repolarization contributes with 13% and gradients along the anatomical axes contribute with 87% to the total gradient in repolarization [5]. Opthof et al. [5] conclude that transmural gradients are not causing the T wave morphology since other gradients have been found to be predominant. Consequently the apico-basal and the anterior-posterior gradients cause dispersion in repolarization [5].

Patel et al. [3] claim that the wedge model preparation provides evidence for a transmural gradient in repolarization. According to Opthof et al. [5], the gradient in repolarization is greater parallel to the endocardium and the epicardium along the apico-basal axis than the transmural gradient in repolarization. However it was shown that isolated areas point out transmural differences [4].
The controversy of the significant gradient in repolarization might result from differences in models. For instance the wedge model preparations differentiate from whole heart preparations. [5]

2.2 Modeling heart tissue

Modelling is an extremely versatile research tool, as it enables the acquisition, deepening and broadening of knowledge about physiological processes [14,16]. Thus, modelling can be used to understand the electrophysiology of human hearts [17]. The variety of cardiac models stretches from molecular to whole heart. This variety is necessary since electrical activity of the heart is influenced by both, microscopic factors, such as ion exchange, and macroscopic factors, such as anisotropic behavior [14,16].

Generally speaking, models are simplified depictions of the complete anatomical and physiological structures, no matter whether considering physiological models in the form of a piece of tissue, e.g. the wedge model (see section 2.3), or theoretical mathematical models, e.g. the bidomain model (see section 4.1) [14]. Mathematical models are mostly computer-based models, hence the increase in

computational power facilitates the use of more detailed, but computational heavier mathematical models. Nonetheless, it is crucial to evaluate the necessary level of detail and the desired efficiency. [1,14]

2.3 Wedge model

A wedge preparation is cut from the ventricular wall of a canine heart in a way that a coronary vessel is parallel and vaguely equally afar from the bottom and top cutting surface [7,9,10]. The size of the wedge preparation varies for left ventricular tissue between $2 \times 1.5 \times 0.9$ and $3 \times 2 \times 1.5$ cm, for right ventricular tissue between $2 \times 1 \times 0.9$ and $2.5 \times 1.5 \times 1.2$ cm [8–10].
Coronary arteries in the wedge preparation are perfused with cardioplegic Tyrode's solution and constant pressure, which is maintained by a roller pump [8,10]. Furthermore the wedge preparation is placed in a physiological bath [7,10].
The endocardium is stimulated in the wedge model [9]. Action potentials are recorded in endocardium, epicardium and midmyocardium via intracellular floating microelectrodes [7,10]. Furthermore an electrode is placed in the bath on each side of the wedge preparation to record an ECG along the transmural axis [7]. Thereby the measured transmural ECG derives from a gradient between endocardium and epicardium [9].
A schematic representation of the wedge model is illustrated in Figure 5.

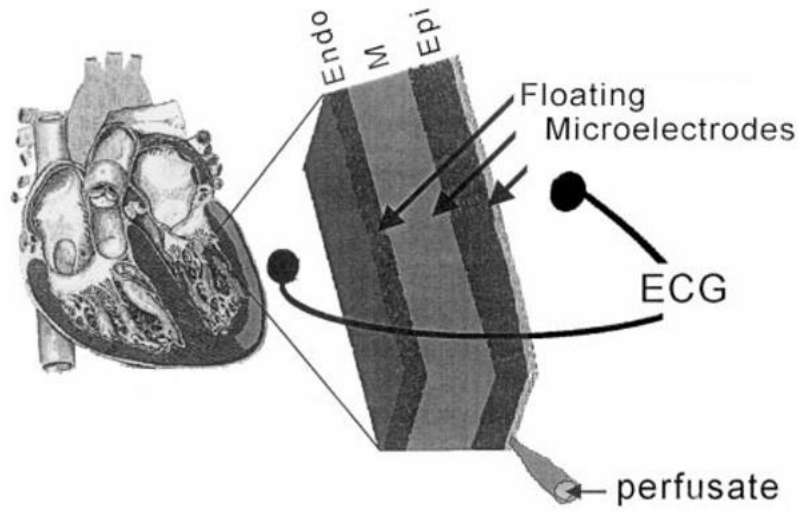

Figure 5: Schematic representation of left ventricular wedge model. (Modified [10].)

Besides wedge preparations of canine hearts, wedge preparations of pig, rabbit and human hearts were examined. However, it is advantageous for wedge models, if the ventricular tissue contains hosts of collateral vessels. Thus the canine heart is, in contrast to human or pig hearts, well suited in the wedge model. [9]

3 Objective

Although ECGs have been used for many years, the emergence of the T wave and details of appurtenant physiological processes are a matter of controversy for decades. [3,4]
T wave genesis has been investigated with an array of experimental heart models [3–6]. Especially wedge preparations from canine hearts showed findings contrary to classical assumptions [3,5,7–10]. However, internal processes within the wedge are not accessible. [11] It is of interest to know, whether findings from the wedge preparation are concordant with physiological electrical behavior of ventricular heart tissue.

Mathematical modelling is an instrument that enables the exploration, acquisition and deepening of knowledge about physiological processes. Thus modelling is a suitable tool to access underlying processes of the wedge preparation. Furthermore it is possible to simulate various conditions with models in order to reconstruct experiments and compare the findings. [14]

The aim of this project was to develop and implement a mathematical bidomain model of a wedge of human left ventricular heart tissue and therewith reconstructing mathematically the setup of a wedge preparation for human tissue.

4 Methods

4.1 Bidomain model

The bidomain model describes the electrical activity of tissue, it is the most complete mathematical description of electrical activity and its propagation and it is validated with animal experiments [18–20,29,30]. Therefore the bidomain model is commonly used and well suited to simulate the electrical activity of the heart on account of its integrity [20,31].

Bidomain modelling is a continuum approach, whereby the electrical activity of the heart is volume-averaged [1,18,19,32]. The cardiac tissue is depicted by intracellular space and extracellular space, superimposed at each considered point [19,29,30,33]. Thus the bidomain model includes two domains, the intracellular domain and the extracellular domain, separated by a membrane [1,19,20,33]. Thereby the membrane works as an electrical insulating boundary, resulting in a volume-averaged potential difference between the intracellular and the extracellular domain. The bidomain model is based on the assumption that current merely pass over from intracellular to extracellular domain across the membrane. [1] Therefore a volume-averaged ionic current model has to be incorporated in the bidomain model to represent the ions passing through the membrane [1,31,33].

In order to incorporate the surroundings of the cardiac tissue and therewith outer influences, the bidomain model is considered to be embedded in an extramyocardial space [1,33]. In the course of this, the intracellular domain persist solely for active tissue, whereas the extracellular domain occurs in active tissue and in the surrounding space, for example a bath [1]. A scheme of a bidomain model and the extramyocardial space is illustrated in Figure 6.

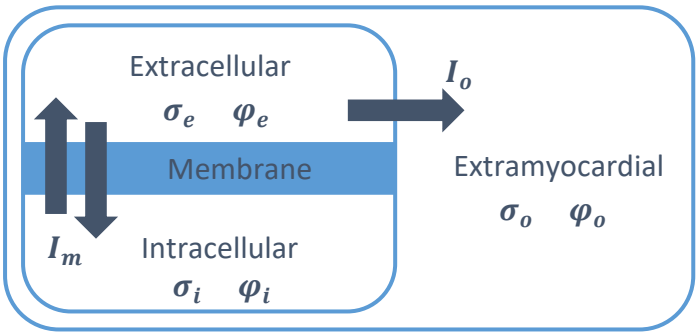

Figure 6: Scheme of bidomain model with intracellular domain (i), extracellular domain (e) and extramyocardial space (o).

The mathematical description of the bidomain model consists of a system of coupled nonlinear partial differential equations [20,29,31,33]. The derivation of the so-called bidomain equations is described in section 4.1.1. Appurtenant boundary conditions for the bidomain model are described in section 4.1.2. Furthermore, considerations for solving the bidomain equations are described in section 4.1.3.

The bidomain modelling approach was used to implement a mathematical description of the left ventricular wedge model and to simulate the electrical activity within the wedge of heart tissue.

4.1.1 Mathematical formulation of the bidomain model

For the mathematical formulation of bidomain model the transmembrane potential V_m is used as starting definition.

$$V_m = \varphi_i - \varphi_e \tag{1}$$

Thereby φ_i denotes the intracellular potential and φ_e the extracellular potential. [1,19,34–36]

According to Ohm's law, current densities J of intra- and extracellular space are given as

$$J_i = -\sigma_i \nabla\varphi_i \tag{2}$$

$$J_e = -\sigma_e \nabla\varphi_e \tag{3}$$

Cardiac tissue is considered as isolated. Therefore the changes in the current density in the intracellular domain are reverse to the changes in the current density in the extracellular domain, which equals the transmembrane current flow.

$$\nabla \cdot (\sigma_i \nabla\varphi_i) = -\nabla \cdot (\sigma_e \nabla\varphi_e) = I_m \tag{4}$$

Thereby σ_i denotes the intracellular conductivity tensor, σ_e the extracellular conductivity tensor and I_m the transmembrane current density per unit area. [1,19,35]

By using Eq. (4) and subtracting $\nabla \cdot (\sigma_i \nabla\phi_e)$ it can be written as

$$\nabla \cdot (\sigma_i \nabla\phi_i) - \nabla \cdot (\sigma_i \nabla\phi_e) = -\nabla \cdot (\sigma_e \nabla\phi_e) - \nabla \cdot (\sigma_i \nabla\phi_e) \tag{5}$$

With Eq. (1) in Eq. (5), it can be written as

$$\nabla \cdot (\sigma_i \nabla V_m) = -\nabla \cdot ((\sigma_i + \sigma_e)\nabla\phi_e) \tag{6}$$

Eq. (6) constitutes the first bidomain equation. [1,19,35,37]

The transmembrane current density I_m can be described with

$$I_m = \beta \left(C_m \frac{\partial V_m}{\partial t} + J_{ion} \right) \tag{7}$$

Thereby β denotes the membrane's surface to volume ratio, C_m the membrane capacitance per unit area and J_{ion} the ionic current density. With Eq. (7) in Eq. (4), it can be written as

$$\nabla \cdot (\sigma_e \nabla \varphi_e) = -\beta \left(C_m \frac{\partial V_m}{\partial t} + J_{ion} \right) \tag{8}$$

Eq. (8) constitutes the second bidomain equation. [1,19]

4.1.2 Boundary conditions

Boundary conditions are applied to regulate the electrical behavior on the edges of domains. Within the bidomain model it is assumed that no current flow occurs between the intracellular domain and the extramyocardial space. Hence the boundary condition of the intracellular domain is written as

$$(\sigma_i \nabla \varphi_i) \cdot n = 0 \qquad x \in \partial H \tag{9}$$

Thereby n denotes a unit vector normal to the tissue boundary and ∂H denotes the outer area of cardiac tissue. [1,19,20,32,34,38,39]

Since the intracellular potential φ_i is not included in the two bidomain equations (6) and (8), Eq. (9) can be written as follows by use of Eq. (1) [1,20,38].

$$(\sigma_i \nabla V_m) \cdot n = (\sigma_i \nabla \varphi_e) \cdot n \qquad x \in \partial H \tag{10}$$

Another boundary condition of the bidomain model is the equilibrium of current flow between the extracellular domain and the extramyocardial space.

$$(\sigma_e \nabla \varphi_e) \cdot n_e = -(\sigma_o \nabla \varphi_o) \cdot n_o \qquad x \in \partial H \tag{11}$$

Thereby σ_o denotes the extramyocardial conductivity tensor and φ_o the extramyocardial potential. n_e denotes the outward unit normal vector from the extracellular domain and n_o denotes the outward unit normal vector from the extramyocardial space, pointing in the opposite direction, hence the sign indicates the direction of current flow. [1,32,38–40]

Furthermore the potential field of the extracellular domain and the extramyocardial space coincide [1,19,20,32,39].

$$\varphi_e = \varphi_o \qquad x \in \partial H \tag{12}$$

Thus, the extramyocardial space, represented by a conductive bath, can be regarded as an add-on to the interstitial (extracellular) fluid [20].

The setup of the model influences the boundaries on the outer edges, i.e. to boundary points next to an electric insulator the no flux, Neumann, boundary condition is applied. [20,33,34,38,40–42]

$$(\sigma_e \nabla \varphi_e) \cdot n = 0 \qquad x \in \partial H \tag{13}$$

Moreover, the Dirichlet boundary condition is applied to the extracellular potential, which is set to zero [19,34,41].

$$\varphi_e = 0 \qquad x \in \partial H \tag{14}$$

4.1.3 Solving bidomain equations

To solve the bidomain equations (6) and (8)

$$\nabla \cdot (\sigma_i \nabla V_m) = -\nabla \cdot ((\sigma_i + \sigma_e)\nabla \phi_e) \tag{6}$$

$$\nabla \cdot (\sigma_e \nabla \varphi_e) = -\beta \left(C_m \frac{\partial V_m}{\partial t} + J_{ion} \right) \tag{8}$$

finite difference method is used, since it is well suited for the simple geometry of the wedge model [34]. The finite difference method is a simple, but exact approach, which requires low memory and is fast to solve [34,41,43].

A finite difference grid is used to represent the tissue and discretize it in order to solve Poisson's equations of the bidomain equations [34,41]. The potential at each point is a function of its neighbor points [41]. For homogeneous conductivity applies

$$\nabla \cdot (\sigma \nabla \varphi) = \sigma \nabla^2 \varphi = \sigma_x \frac{\partial^2 \varphi}{\partial x^2} + \sigma_y \frac{\partial^2 \varphi}{\partial y^2} + \sigma_z \frac{\partial^2 \varphi}{\partial z^2} \tag{15}$$

The finite difference method approximates the solution of differential equations by using the finite differences of the neighboring node points [34,41,44]. This is implemented by a Laplacian matrix, which constitutes the operator $\nabla \cdot (\sigma \nabla)$. In the Laplacian matrix anisotropy is considered and the boundary conditions are included. [37] The influence of the neighboring grid points in the finite difference method is illustrated in Figure 7.

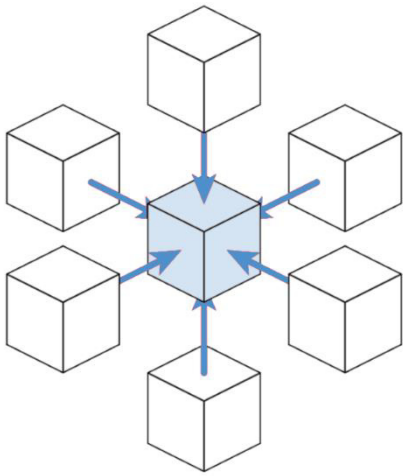

Figure 7: Illustration of the influence of neighboring points by using the finite difference method. In order to approximate the solution of a node point, finite differences of all 6 neighbor points are considered. (Modified [45].)

A linear system of algebraic equations arises from the spatial discretization, which needs to be solved at each time step [31]. Sufficient three-dimensional discretization commonly requires a large quantity of node points, as the node points should be approximately 0.1 to 0.2 mm distant. This, in turn, requires greatly increased memory and therewith more processing power. Hence, the feasible size as well as the simulation time of the model is limited by the available computational resources, in spite of its low computational requirements, as compared with, e.g., finite element method. [18,20,30,31,41] Therefore sparse matrixes were employed to alleviate computational demands.

The system of linear algebraic equations resulting from the finite difference method may be solved by any standard approach, which is suitable for sparse matrixes [41]. Direct solvers are more accurate than iterative methods, however direct solvers have larger memory requirements [20,42]. I.e. large matrixes in linear algebraic systems are an issue for the efficiency of direct solvers, since the number of operations accelerate with rising number of entries per row. The largest bidomain models solved directly were solely composed of a few millions of node points in total. [20] That is, considering the necessary spatial discretization, a relatively small number. Hence, with an increasing number of node points iterative approaches become necessary, as direct solvers are not efficient enough with respect to memory and time. Iterative solvers approximate the solution by minimizing the residual. [42]
Since iterative solvers are necessary to solve a descriptively sized bidomain model efficiently, but provide less accurate solutions, the solver must be chosen wisely. Therefore the backslash operator, a direct solver, was used for a low scale grid bidomain model. The preconditioned conjugate gradient method and the biconjugate gradient stabilized method were used for the same low scale grid bidomain model. The solutions of those iterative solvers were compared to the accurate solution. The decision was made based on discrepancy from the accurate solution.

4.2 Ionic current model

Cardiac cell models are used to provide insight into the electrical activity of single cells across the membrane [1,12,13]. The governed action potential displays the potential gradient across the cell membrane. Cardiac cell models range from simple models to biophysical detailed models. [1] Simplified models provide action potentials with low computational cost. This is possible as the underlying physiological processes are neglected, and solely the fundamental properties of the action potential are considered. [1,46]
Biophysical detailed models on the other hand describe the electrical activity of a cardiac cell more accurately by including the underlying mechanisms of the potential gradient across the membrane, like the ion flow via pumps, channels or exchangers. An example for this is the Ten Tusscher model, which includes detailed description of the major ionic currents and intracellular calcium, sodium and potassium dynamics, governed from measurements of human hearts. [1,12,47] A schematic representation of the ionic dynamics in the Ten Tusscher model is illustrated in Figure 8.

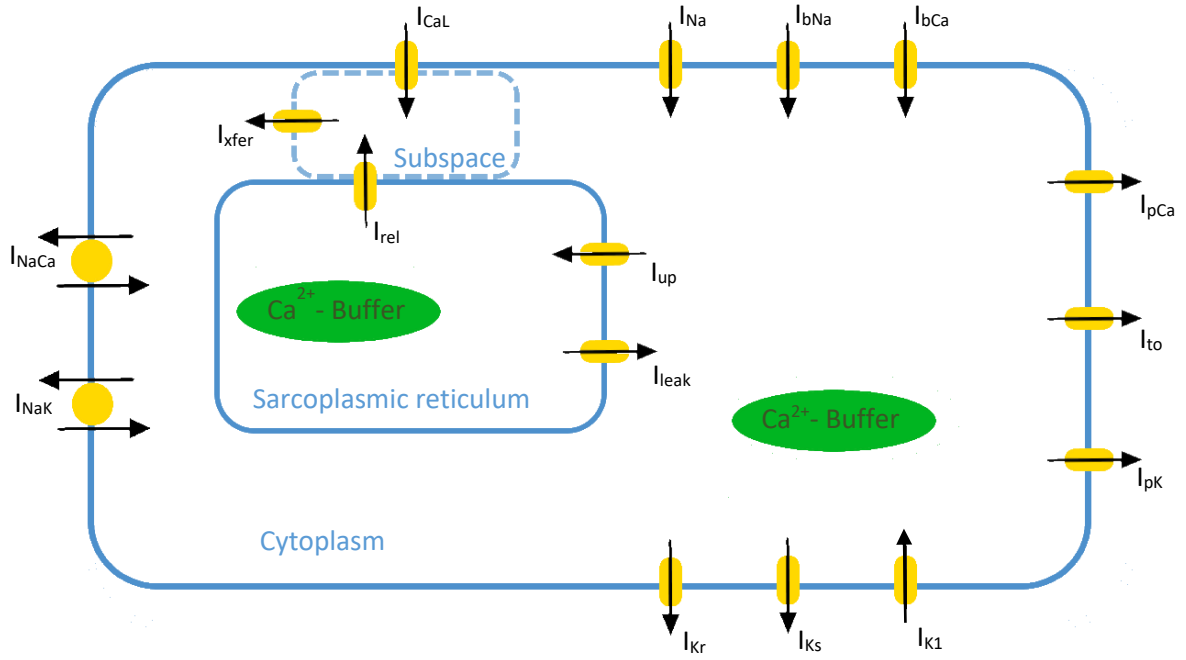

Figure 8: Schematic representation of ionic currents, exchangers and pumps in the Ten Tusscher model. I_{Na}: Na^+ current; I_{bNa}: background Na^+ current; I_{bCa}: background Ca^{2+} current; I_{pCa}: sarcolemmal Ca^{2+} pump current; I_{to}: transient outward curret; I_{pK}: plateau K^+ current; I_{K1}: inward rectifier K^+ current; I_{Ks}: slow delayed rectifier current; I_{Kr}: rapid delayed rectifier current; I_{NaK}: Na^+-K^+ pump current; I_{NaCa}: Na^+/Ca^{2+} exchanger current; I_{CaL}: L-type Ca^{2+} current; I_{xfer}: diffusive Ca^{2+} current between subspace and cytoplasm; I_{rel}: Ca^{2+}- induced Ca^{2+} release current; I_{up}: sarcoplasmic reticulum Ca^{2+} pump current; I_{leak}: sarcoplasmic reticulum Ca^{2+} leak current.

For applicability of the bidomain model, an ionic current model must be incorporated to describe membrane dynamics of modeled tissue [18,20]. As mentioned above, an ionic current model describes the chemical and electrical gradients across the cell membrane of a single cardiac cell by simulating the subcellular processes as the selective permeability of the cell membrane for distinct ions under different conditions. However, by incorporating an ionic current model into the bidomain model, it must be taken into account that the units might differ between both. [1]

The chosen model in order to incorporate ionic currents in the bidomain model was the Ten Tusscher model, which models the major ionic currents based on experimental data [12,47]. Since it is describing subcellular ionic dynamics like ionic currents and pumps in single human epicardial, midmyocardial and endocardial ventricular cells, the Ten Tusscher model is suitable to incorporate into the bidomain model [1,12,47].

Admittedly the bidomain model is extremely computational heavy due to the necessary discretization and the detailed incorporated ionic current model [18,31,42]. Therefore simplification in the form of the reduced Ten Tusscher model was applied until complete implementation of the bidomain model in order to use the available computational power more efficient.
The reduced version of the Ten Tusscher model is of less detailed and therefore computationally four times more efficient than the full model. Similar to the full model, the reduced version describes changes of ionic currents and ion channels. Nevertheless, the reduced Ten Tusscher model shows a similar action potential morphology and is equally suited for ionic simulations. [13]

4.3 Simulating the electrical activity of wedge of heart tissue

The experimental wedge model (see section 2.3), is reconstructed mathematically. Therefore a wedge of left ventricular tissue is described with the bidomain model. The wedge of heart tissue is surrounded by a conductive bath. A schematic description of the setup is illustrated in Figure 9.

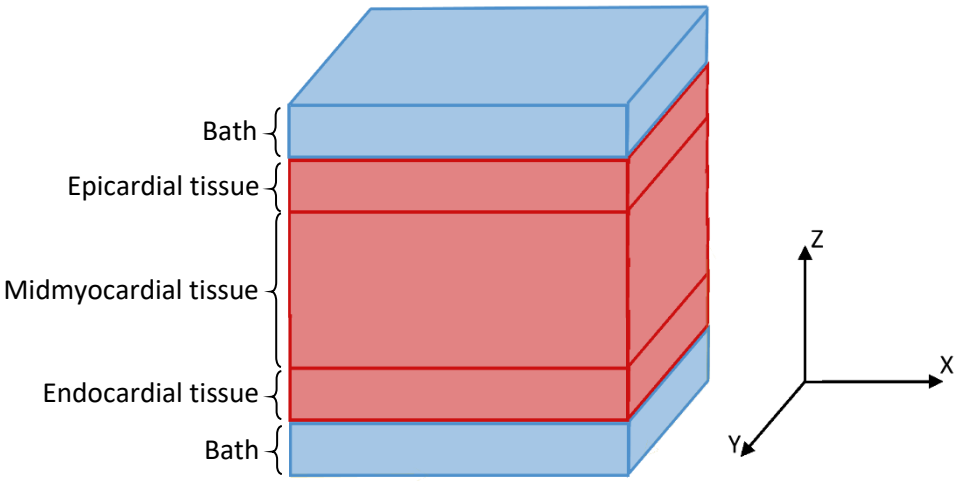

Figure 9: Configuration of the bidomain model for simulating wedge preparations.

A stimulus current is applied in one node point in the endocardial tissue. The development and progression of the electrical activity, triggered by the stimulus, is simulated with the bidomain model. An ECG is calculated across the wedge and compared to the ones recorded from a wedge preparation.

5 Results

5.1 Bidomain model

The bidomain model for simulating the electrical activity of a wedge of heart tissue, surrounded by a conducting bath, was implemented in MATLAB. It enables to gauge the membrane potentials in each node point of the tissue, and the extracellular potentials in all node points of the bath and the tissue. The work flow of the model is illustrated by the flowchart in Figure 10 and explained in detail down below.

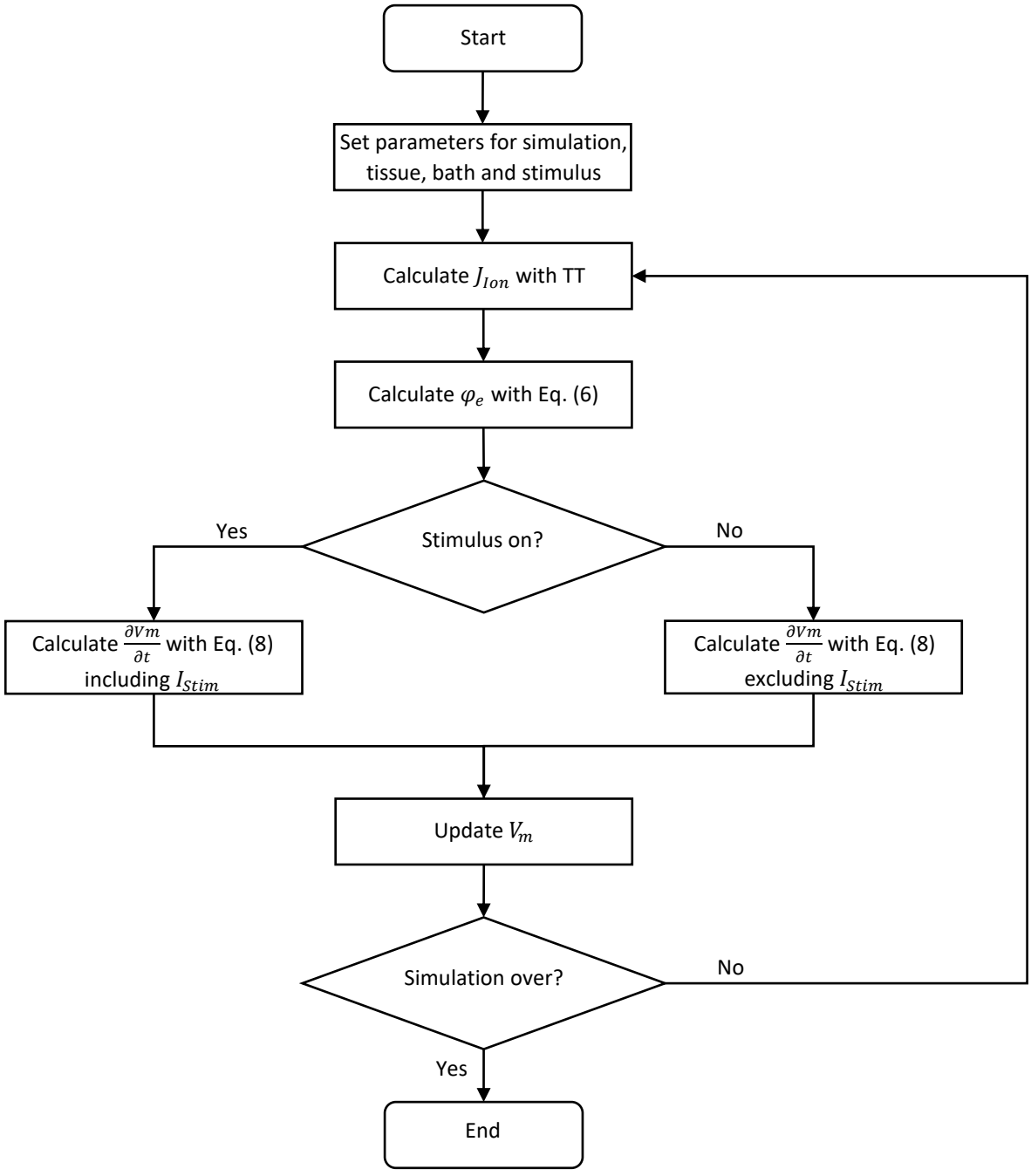

Figure 10: Work flow of the implemented bidomain model. Here TT abbreviates Ten Tusscher model.

The parameters for bath and tissue are initialized. Thereby properties of endocardial, midmyocardial and epicardial cells are considered, in order to mimic ventricular tissue appropriately. Furthermore the simulation time as well as the stimulus point and duration are edited. Sparse Laplacian matrixes are set to facilitate solving the linear algebraic systems originating form the finite difference method approach. The parameter setting is listed in Table 1.

Table 1: Parameter setting of implemented bidomain model.

Parameter	Description	Value
Δt	Size of time step (temporal discretization)	$0.02\ ms$
h	Distance between node points (spatial discretization)	$0.2 * 10^{-3} m$
$\sigma_{i,x}$	Intracellular conductivity along fibers	$0.2\ \frac{S}{m}$
$\sigma_{i,y}$	Intracellular conductivity perpendicular fibers	$0.02\ \frac{S}{m}$
$\sigma_{i,z}$	Intracellular conductivity perpendicular fibers	$0.02\ \frac{S}{m}$
$\sigma_{e,x}$	Extracellular conductivity along fibers	$0.2\ \frac{S}{m}$
$\sigma_{e,y}$	Extracellular conductivity perpendicular fibers	$0.08\ \frac{S}{m}$
$\sigma_{e,z}$	Extracellular conductivity perpendicular fibers	$0.08\ \frac{S}{m}$
σ_b	Conductivity of bath	$0.2 \frac{S}{m}$
β	Surface area to volume ratio	$3 * 10^5\ \frac{1}{m}$
C_m	Membrane capacitance per unit surface area	$10^{-2} \frac{F}{m^2}$
$V_{m,t=0}$	Initial membrane potential	$-86{,}2 * 10^{-3}\ V$
I_{Stim}	Stimulus current	$150 \frac{mA}{m^2}$

The Ten Tusscher model was incorporated to yield the ionic current density J_{Ion}. The parameters thereof are not listed in Table 1, since relevant details can be found in the original publication of Ten Tusscher et al. [47].

The first bidomain equation (6) is used to calculate the extracellular potential φ_e. This linear algebraic system is solved with the biconjugate gradient stabilized method, which was chosen after an accuracy test. The obtained extracellular potential φ_e is used to calculate $\frac{\partial V_m}{\partial t}$ with the second bidomain equation (8). If the stimulus is still on, the stimulus current I_{Stim} is included in the calculation. Obtained $\frac{\partial V_m}{\partial t}$ is used to update the membrane potential V_m with the Euler method. Until the end of the simulation is reached, this is repeated for every time step from calculating the ionic current density J_{Ion} to updating the membrane potential V_m.

The full MATLAB script of the bidomain model for simulating the electrical activity of a wedge of left ventricular heart tissue can be found in Appendix A.

5.2 Simulating the electrical activity of wedge of heart tissue

Unfortunately, the implemented bidomain model failed to simulate the electrical activity in the setup of a wedge preparation for human tissue. In fact, electrical activity was generated, however the generated action potentials did not amount to physiological electrical behavior. The obtained action potentials are illustrated in Figure 11.

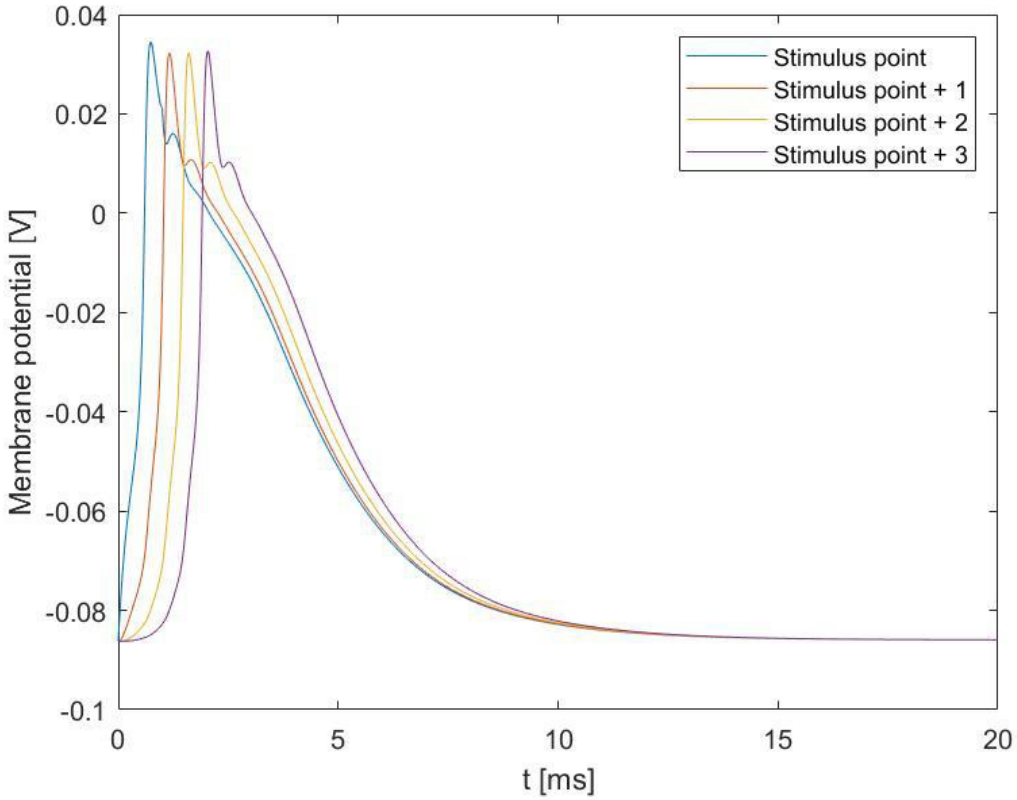

Figure 11: Membrane potentials in stimulus point and three adjacent points after stimulation.

The blue graph illustrates the membrane potential in the stimulus point. Red, yellow and purple graphs illustrate the membrane potentials in the node points one, two and three adjacent to the stimulus point. Electrical activity can be observed in all displayed points. The delay in the changes of the membrane potentials are due to propagation through the tissue. However, obtained membrane potentials do not fulfill the expectations of a physiological action potential. Those membrane potentials mimic the general shape of an action potential in a fraction of the physiological action potential duration. Hence it is assumed that the implemented bidomain model contains an error, causing the non-physiological behavior of the membrane after excitation. In order to determine the source of the error, several tests were conducted.

It has been reviewed, if both bidomain equations and the Laplacian matrixes have been implemented correctly. Different solvers for linear algebraic system, backslash operator, biconjugate gradient stabilized method and preconditioned conjugated gradient method, were compared. The influence of the boundary conditions and the surrounding bath were tested. Furthermore, it was tested, if the model is working without coupling the neighboring cells. Thereby a stimulus was applied to one single cell and a proper action potential, as illustrated in Figure 12, was generated.

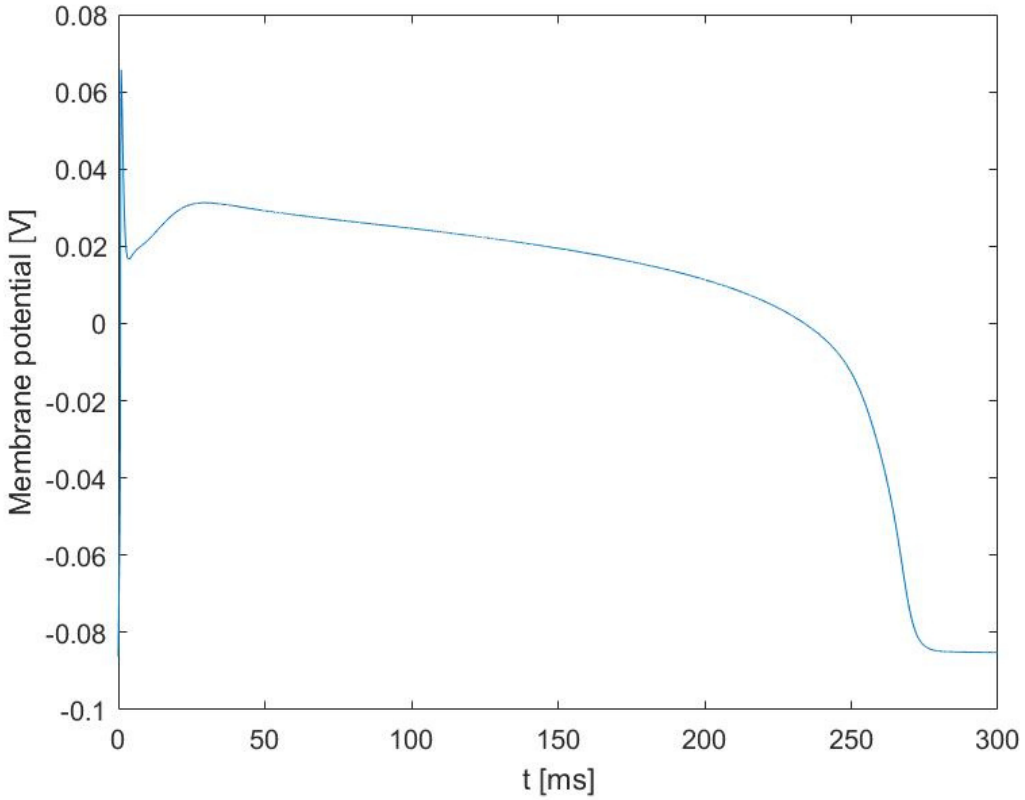

Figure 12: Membrane potential in the stimulus point after decoupling neighboring cells.

It was revised, if the units throughout the bidomain model coincide. Moreover, it was switched to the monodomain model (see Appendix B), which is solely considering the intracellular domain. Finally, various possible values for the parameters, presented in Table 1, were examined.

In order to examine whether the occurring error is caused by the Ten Tusscher model, another ionic model, the Beeler-Reuter model, was incorporated into the monodomain model. With the incorporated Beeler-Reuter model electrical activity was generated, however the generated electrical activity did not amount to physiological electrical behavior. The obtained action potentials are illustrated in Figure 13.

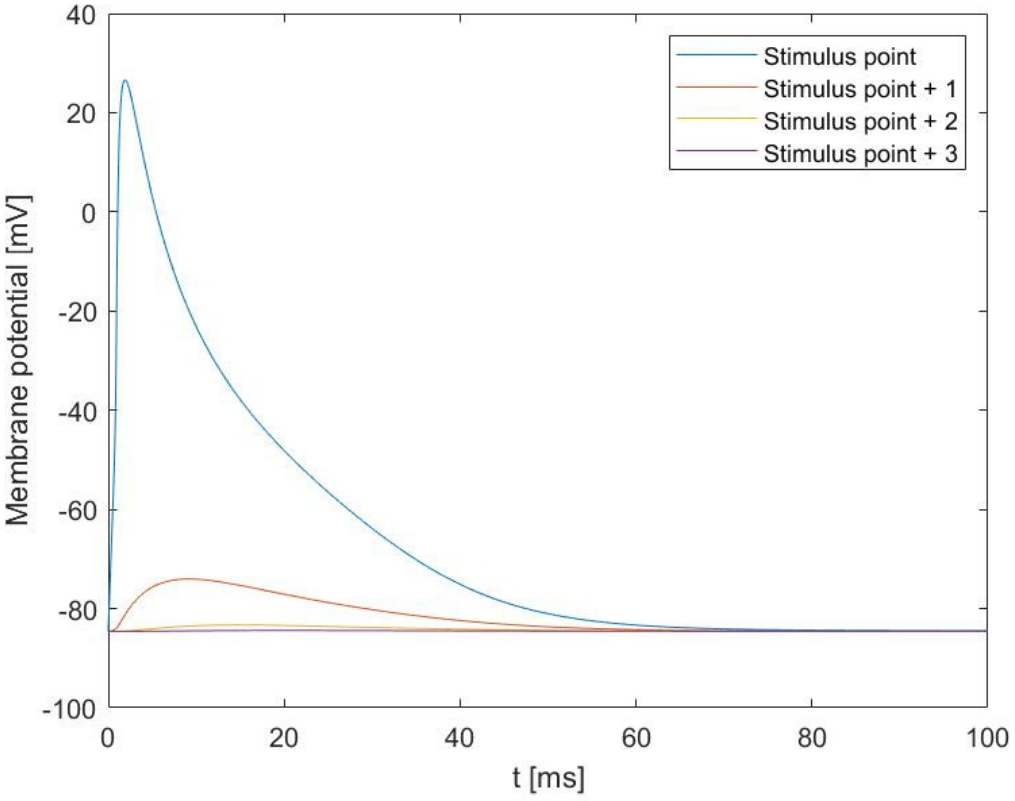

Figure 13: Membrane potential in stimulus point and three adjacent points after stimulation.

The blue graph illustrates the membrane potential in the stimulus point. Red, yellow and purple graphs illustrate the membrane potentials in the node points one, two and three adjacent to the stimulus point. Electrical activity can be observed in the stimulus point and marginally in the node points one and two next to the stimulus point. The delay in the start of the electrical activity is due to its propagation through the tissue. However, the obtained electrical activity does constitute a physiological action potential.

Since the implemented model with incorporation of the Ten Tusscher model generated a proper action potential after decoupling the neighboring cells, it was tested, if the model with incorporation of the Beeler-Reuter model shows the same behavior after decoupling the neighboring cells. A stimulus was applied to one single cell and generated a proper action potential, as illustrated in Figure 14.

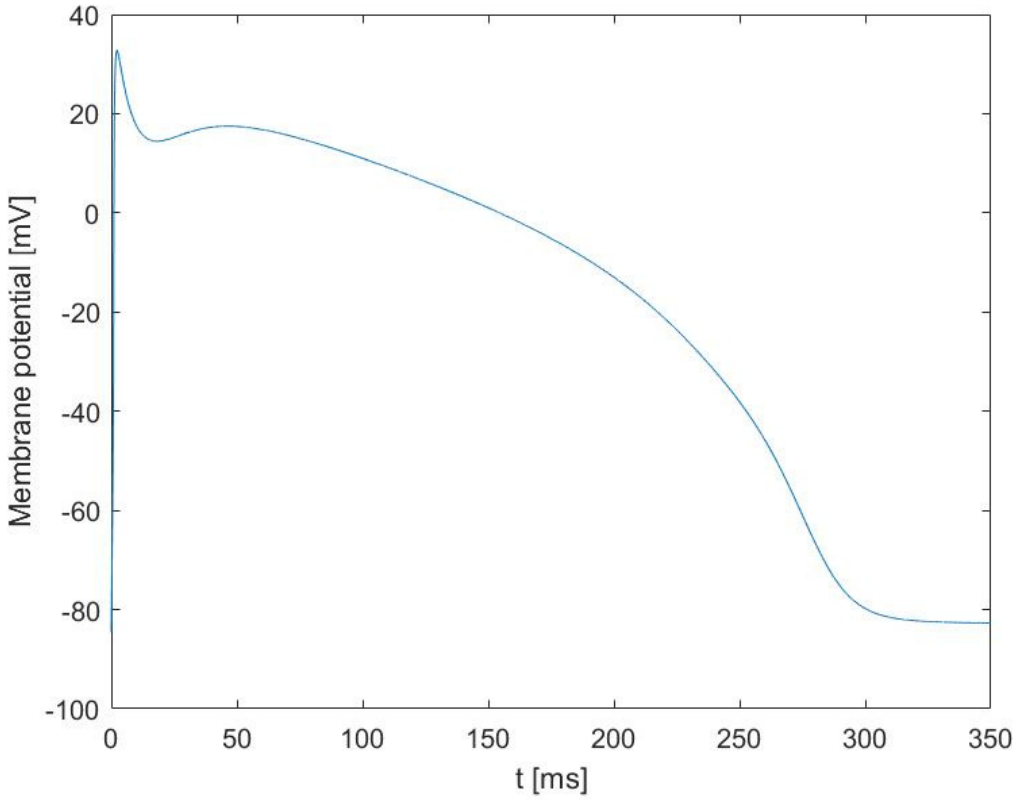

Figure 14: Membrane potential in the stimulus point after decoupling neighboring cells, generated with a monodomain model with incorporated Beeler-Reuter model.

It can be observed that this model generates a different action potential morphology than the incorporation of the Ten Tusscher model. The reason for this is solely the differences within the ionic current models.

In the monodomain model with the incorporation of the Beeler-Reuter model, too, different parameter settings were examined.
However, all measures did not improve the performance of the implemented model.

6 Discussion

6.1 Bidomain model

A bidomain model was implemented to mathematically reconstruct the setup of a wedge preparation for human tissue and simulate the electrical activity in the wedge. Bidomain models, solved by finite difference method, are a suitable approach to model the electrical activity of tissue. However a limitation of the bidomain model are its computational needs, which is limiting the size of the feasible finite difference grid and therewith the size of the model [33,41].
Furthermore larger tissue wedges engender an extensive linear system, which cannot be solved with the accurate direct solvers. The use of less accurate iterative methods may affect the conciseness of the simulated electrical activity.
In literature, there is no concordance of the applied parameters, for instance the intracellular and extracellular conductivity values as well as the unit surface area to volume. Resulting variations might also affect the conciseness of the simulated electrical activity.

6.2 Simulating the electrical activity of wedge of heart tissue

Against expectation, the implemented bidomain model failed to simulate the electrical activity in the setup of a wedge preparation for human tissue. Either propagation of electrical activity through the tissue or a proper action potential could be achieved, but not both at the same time. Since the Ten Tusscher model incorporated in the bidomain as well as in the monodomain model, and the Beeler-Reuter model incorporated in the monodomain model were able to generate action potentials in the case of uncoupled neighboring cells, but were not able to generate action potentials in the case of coupled neighboring cells, it is assumed that the coupling of the neighboring cells is the source of the error. The question arises, whether a coupling variable is necessary. However, studies which combined the bidomain model with the Ten Tusscher or the Beeler-Reuter model do not indicate this.

Sambelashvili et al. [48] state that it is possible to shorten the action potential by accelerating the slow inward calcium current in the Beeler-Reuter model. In the course of unit testing the reversion of this, i.e. inhibiting of the calcium current was examined. As a result of this, the shape of the action potential in the stimulus point improved, but not in terms of propagation. Those observations strengthen the suspicion that the coupling of the neighboring cells is causing the error.

One might claim, that the coupling is implemented wrong. The Laplacian matrixes, which are used to calculate the finite differences of the neighboring points and therewith determining the coupling, have been revised and found correctly implemented. Thus, again the question arises, whether there is a coupling variable necessary. But as mentioned before, studies which combined the bidomain model with the Ten Tusscher or the Beeler-Reuter model do not indicate this.

7 Conclusion

The implemented mathematical bidomain model of a wedge of human left ventricular heart tissue failed to simulate the electrical activity in the setup of a wedge preparation for human cardiac tissue.

Either propagation of electrical activity through the tissue or a proper action potential could be achieved, but not both simultaneously. It is assumed that the coupling of the neighboring cells in the bidomain model is causing this present problem.

Thus further investigation is necessary, in order to eliminate the source of error and improve the coupling of the neighboring cells. Therewith a full working order of the bidomain model of a wedge of human heart tissue can be achieved, and the electrical activity in the setup of a wedge preparation of human tissue can be simulated.

References

[1] A. J. Pullan, L. K. Cheng, and M. L. Buist, *Mathematically modelling the electrical activity of the heart*: *From cell to body surface and back again*, World Scientific, New Jersey u.a, 2005.

[2] P. W. Macfarlane, *Comprehensive electrocardiology*: *Theory and practice in health and disease*, Springer, New York, London, 2010.

[3] C. Patel, J. F. Burke, H. Patel et al., "Is there a significant transmural gradient in repolarization time in the intact heart? Cellular basis of the T wave: a century of controversy," *Circulation. Arrhythmia and electrophysiology*, vol. 2, no. 1, pp. 80–88, 2009.

[4] V. M. F. Meijborg, C. E. Conrath, T. Opthof et al., "Electrocardiographic T wave and its relation with ventricular repolarization along major anatomical axes," *Circulation. Arrhythmia and electrophysiology*, vol. 7, no. 3, pp. 524–531, 2014.

[5] T. Opthof, R. Coronel, and M. J. Janse, "Is there a significant transmural gradient in repolarization time in the intact heart? Repolarization Gradients in the Intact Heart," *Circulation. Arrhythmia and electrophysiology*, vol. 2, no. 1, pp. 89–96, 2009.

[6] J. Burdon-Sanderson, "On the Electrical Phenomena of the Excitatory Process in the Heart of the Frog and of the Tortoise, as investigated Photographically," *The Journal of physiology*, vol. 4, no. 6, 327-386.15, 1884.

[7] C. Antzelevitch, "Role of transmural dispersion of repolarization in the genesis of drug-induced torsades de pointes," *Heart rhythm*, vol. 2, 2 Suppl, S9-15, 2005.

[8] J. M. Di Diego and C. Antzelevitch, "Cellular basis for ST-segment changes observed during ischemia," *Journal of Electrocardiology*, vol. 36, pp. 1–5, 2003.

[9] J. M. Di Diego, S. Sicouri, R. C. Myles et al., "Optical and electrical recordings from isolated coronary-perfused ventricular wedge preparations," *Journal of molecular and cellular cardiology*, vol. 54, pp. 53–64, 2013.

[10] G.-X. Yan, W. Shimizu, and C. Antzelevitch, "Characteristics and Distribution of M Cells in Arterially Perfused Canine Left Ventricular Wedge Preparations," *Circulation*, vol. 98, no. 18, pp. 1921–1927, 1998.

[11] E. A. Heidenreich, J. F. Rodríguez, F. J. Gaspar et al., "Fourth-order compact schemes with adaptive time step for monodomain reaction–diffusion equations," *Journal of Computational and Applied Mathematics*, vol. 216, no. 1, pp. 39–55, 2008.

[12] K. H. W. J. ten Tusscher, D. Noble, P. J. Noble et al., "A model for human ventricular tissue," *American journal of physiology. Heart and circulatory physiology*, vol. 286, no. 4, H1573-89, 2004.

[13] K. H. W. J. ten Tusscher and A. V. Panfilov, "Cell model for efficient simulation of wave propagation in human ventricular tissue under normal and pathological conditions," *Physics in medicine and biology*, vol. 51, no. 23, pp. 6141–6156, 2006.

[14] F. B. Sachse, *Computational Cardiology*: *Modeling of Anatomy, Electrophysiology, and Mechanics*, Springer, Berlin, Heidelberg, 2004.

[15] C. S. Henriquez, A. L. Muzikant, and C. K. Smoak, “Anisotropy, Fiber Curvature, and Bath Loading Effects on Activation in Thin and Thick Cardiac Tissue Preparations,” *Journal of cardiovascular electrophysiology*, vol. 7, no. 5, pp. 424–444, 1996.

[16] N. Cusimano and L. Gerardo-Giorda, “A space-fractional Monodomain model for cardiac electrophysiology combining anisotropy and heterogeneity on realistic geometries,” *Journal of Computational Physics*, vol. 362, pp. 409–424, 2018.

[17] Balakrishnan M., Chakravarthy S., and Guhathakurta S., “A Simple 2D Whole Heart Model for Simulating Electrocardiograms,” *Computing in Cardiology*, pp. 517–520, 2014.

[18] L. Pegolotti, L. Dedè, and A. Quarteroni, “Isogeometric Analysis of the electrophysiology in the human heart: Numerical simulation of the bidomain equations on the atria,” *Computer Methods in Applied Mechanics and Engineering*, vol. 343, pp. 52–73, 2019.

[19] S. M. Kandel, “The Electrical Bidomain Model: A Review,” *Scholars Academic Journal of Biosciences (SAJB)*, vol. 3, no. 7, pp. 633–639, 2015.

[20] E. J. Vigmond, R. Weber dos Santos, A. J. Prassl et al., “Solvers for the cardiac bidomain equations,” *Progress in biophysics and molecular biology*, vol. 96, 1-3, pp. 3–18, 2008.

[21] J. Malmivuo and R. Plonsey, *BioelectromagnetismPrinciples and Applications of Bioelectric and Biomagnetic Fields*, Oxford University Press, 1995.

[22] “#18131928,” Colorbox, https://www.colourbox.com/image/ecg-graph-image-18131928.

[23] W. M. Bayliss and E. H. Starling, “On the electromotive phenomena of the mammalian heart,” *Proceedings of the Royal Society of London*, vol. 50, 302-307, pp. 211–214, 1892.

[24] G. R. Mines, “On functional analysis by the action of electrolytes,” *The Journal of physiology*, vol. 46, no. 3, pp. 188–235, 1913.

[25] M. S. Spach and R. C. Barr, “Anaylsis of ventricular activation and repolarization from intramural and epicardial potential distributions for ectopic beats in the intact dog,” *Circulation Research*, vol. 37, no. 6, pp. 830–843, 1975.

[26] M. R. Franz, K. Bargheer, W. Rafflenbeul et al., “Monophasic action potential mapping in human subjects with normal electrocardiograms: direct evidence for the genesis of the T wave,” *Circulation*, vol. 75, no. 2, pp. 379–386, 1987.

[27] S. Sicouri and C. Antzelevitch, “A subpopulation of cells with unique electrophysiological properties in the deep subepicardium of the canine ventricle. The M cell,” *Circulation Research*, vol. 68, no. 6, pp. 1729–1741, 1991.

[28] E. N. Moore, J. B. Preston, and G. K. Moe, “Durations of Transmembrane Action Potentials and Functional Refractory Periods of Canine False Tendon and Ventricular Myocardium,” *Circulation Research*, vol. 17, no. 3, pp. 259–273, 1965.

[29] B. J. Roth, “How the anisotropy of the intracellular and extracellular conductivities influences stimulation of cardiac muscle,” *Journal of Mathematical Biology*, vol. 30, no. 6, 1992.

[30] M. Potse, B. Dubé, J. Richer et al., “A comparison of monodomain and bidomain reaction-diffusion models for action potential propagation in the human heart,” *IEEE transactions on bio-medical engineering*, vol. 53, 12 Pt 1, pp. 2425–2435, 2006.

[31] J. Sundnes, B. F. Nielsen, K. A. Mardal et al., “On the computational complexity of the bidomain and the monodomain models of electrophysiology,” *Annals of Biomedical Engineering*, vol. 34, no. 7, pp. 1088–1097, 2006.

[32] B. J. Roth, “A comparison of two boundary conditions used with the bidomain model of cardiac tissue,” *Annals of Biomedical Engineering*, vol. 19, no. 6, pp. 669–678, 1991.

[33] H. I. Saleheen, P. D. Claessen, and K. T. Ng, “Three-dimensional finite-difference bidomain modeling of homogeneous cardiac tissue on a data-parallel computer,” *IEEE transactions on bio-medical engineering*, vol. 44, no. 2, pp. 200–204, 1997.

[34] M. Buist, G. Sands, P. Hunter et al., “A Deformable Finite Element Derived Finite Difference Method for Cardiac Activation Problems,” *Annals of Biomedical Engineering*, vol. 31, no. 5, pp. 577–588, 2003.

[35] D. B. Geselowitz and W. T. Miller, “A bidomain model for anisotropic cardiac muscle,” *Annals of Biomedical Engineering*, vol. 11, 3-4, pp. 191–206, 1983.

[36] N. Hooke, C. S. Henriquez, P. Lanzkron et al., “Linear algebraic transformations of the bidomain equations: implications for numerical methods,” *Mathematical biosciences*, vol. 120, no. 2, pp. 127–145, 1994.

[37] A. D. Fitt, J. Norbury, H. Ockendon et al., *Progress in Industrial Mathematics at ECMI 2008 // Framework for Modular, Flexible and Efficient Solving the Cardiac Bidomain Equations Using PETSc*, Springer Berlin Heidelberg, Berlin, Heidelberg, 2010.

[38] M. L. Trew, B. H. Smaill, D. P. Bullivant et al., “A generalized finite difference method for modeling cardiac electrical activation on arbitrary, irregular computational meshes,” *Mathematical biosciences*, vol. 198, no. 2, pp. 169–189, 2005.

[39] B. J. Roth, “Action potential propagation in a thick strand of cardiac muscle,” *Circulation Research*, vol. 68, no. 1, pp. 162–173, 1991.

[40] N. Trayanova and G. Plank, “Bidomain Model of Defibrillation,” in *Cardiac Bioelectric Therapy,* I. R. Efimov, M. W. Kroll, and P. J. Tchou, Eds., pp. 85–109, Springer US, Boston, MA, 2009.

[41] H. I. Saleheen and K. T. Ng, “New finite difference formulations for general inhomogeneous anisotropic bioelectric problems,” *IEEE transactions on bio-medical engineering*, vol. 44, no. 9, pp. 800–809, 1997.

[42] R. Weber dos Santos, G. Plank, S. Bauer et al., “Parallel multigrid preconditioner for the cardiac bidomain model,” *IEEE transactions on bio-medical engineering*, vol. 51, no. 11, pp. 1960–1968, 2004.

[43] B. E. Rapp, “Finite Difference Method,” in *Microfluidics: Modelling, Mechanics and Mathematics*, pp. 623–631, Elsevier, 2017.

[44] J. O. Dow, “Elements of the Finite Difference Method,” in *A Unified Approach to the Finite Element Method and Error Analysis Procedures*, pp. 317–349, Elsevier, 1999.

[45] Gentryx, “Model of the stencil defined by the von Neumann neighborhood in 3D,” https://commons.wikimedia.org/wiki/File:3D_von_Neumann_Stencil_Model.svg.

[46] B. Xu, S. Binczak, S. Jacquir et al., “Parameters analysis of FitzHugh-Nagumo model for a reliable simulation,” *Conference proceedings : … Annual International Conference of the IEEE*

Engineering in Medicine and Biology Society. IEEE Engineering in Medicine and Biology Society. Annual Conference, vol. 2014, pp. 4334–4337, 2014.

[47] K. H. W. J. ten Tusscher and A. V. Panfilov, “Alternans and spiral breakup in a human ventricular tissue model,” *American journal of physiology. Heart and circulatory physiology*, vol. 291, no. 3, H1088-100, 2006.

[48] A. Sambelashvili and I. R. Efimov, “Dynamics of virtual electrode-induced scroll-wave reentry in a 3D bidomain model,” *American journal of physiology. Heart and circulatory physiology*, vol. 287, no. 4, H1570-81, 2004.

Appendix A

Full MATLAB code of the bidomain model for simulating the electrical activity of a wedge of left ventricular human heart tissue.

```
%% 3D model - bidomain - TT

clc
clearvars;

%% Tissue Grid
Tx = 50;        % grid length in x direction
Ty = 50;        % grid length in y direction
Tz = 50;        % grid length in z direction
TS = Tx*Ty*Tz;  % Tissue size
ht = 0.2e-3;    % distance between tissue grid points [m]

endo = Tx*Ty*(1e-3/ht);        % last grid point of endocardial tissue
myo = endo+Tx*Ty*(8e-3/ht);    % last grid point of mid-myocardial tissue
epi = myo+Tx*Ty*(1e-3/ht);     % last grid point of epicardial tissue

%% Bath grid (on two sides of tissue)
Bx = Tx;        % grid length in x direction
By = Ty;        % grid length in y direction
Bz = 10;        % grid length in z direction
BS = Bx*By*Bz;  % Bath size (on each side of tissue)
hb = 0.2e-3;       % distance between bath grid points [m]

%% Time steps
t_simulation = 300;         % simulation time [ms]
delta_t = 0.02;             % size of time step [ms]
N = t_simulation/delta_t;   % number of time steps

%% Stimulus
Stimulus = 150;   % stimulus current [mA/m^2]
t_stim_on = 5;       % sart of stimulus [ms]
t_stim = 1;          % stimulus duration [ms]
t_stim_on =t_stim_on/delta_t;
t_stim = t_stim/delta_t;

x = 10;     % x position of stimulus point
y = 7;     % y position of stimulus point
z = 4;      % z position of stimulus point

P = x+(y-1)*Tx+(z-1)*Tx*Ty; % calculation of stimuluspoint number
Istim = zeros(TS,1);
Istim(P,1) = Stimulus;

%% Membrane parameters
Cm = 1e-2;      % capacitance [F/m^2]
beta = 3e5;     % surface to volume ratio [1/m]

% Conductivity
sigmax_i = 0.2;     % intracell. along fibre (x dir.) [S/m]
sigmay_i = 0.02;    % intracell. vertical to fibre (y dir.) [S/m]
sigmaz_i = 0.02;    % intracell. vertical to fibre (z dir.) [S/m]
sigmax_e = 0.2;     % extracell. along fibre (x dir.) [S/m]
sigmay_e = 0.08;    % extracell. vertical to fibre (y dir.) [S/m]
sigmaz_e = 0.08;    % extracell. vertical to fibre (z dir.) [S/m]
sigmax_b = 0.2;    % bath in x direction [S/m]
sigmay_b = 0.2;    % bath in y direction [S/m]
sigmaz_b = 0.2;    % bath in z direction [S/m]

% Laplacian Matrixes
% If simulations with the same grid size are conducted several times,
% it is suggested to save the matrixes and only load them.
% Boundary conditions are included in the matrixes.

% Laplacian matrix for sigma_i in tissue and bath
BigM_i = spalloc(TS+2*BS,TS+2*BS,2*Tx*Ty+2*(Ty-2)*(Tz-2)+6*(Tx-2)*(Ty-2)*(Tz-2)+2*BS);
for n = 1:BS
    BigM_i(n,n) = 1;
end
for n = BS+1:BS+TS
    BigM_i(n,n) = 1;
    if n < BS+Tx*Ty+1
        for k = 1:Ty-2
        if n > BS+k*Tx+1 && n < BS+(k+1)*Tx
        BigM_i(n,n) = (-2*sigmax_i-2*sigmay_i)/ht^2;
        BigM_i(n,n-1) = sigmax_i/ht^2;
        BigM_i(n,n+1) = sigmax_i/ht^2;
        BigM_i(n,n-Tx) = sigmay_i/ht^2;
        BigM_i(n,n+Tx) = sigmay_i/ht^2;
        end
        end
```

```
    end
    for kk = 1:Tz-2
        for k = 1:Ty-2
            if ((n > BS+kk*Tx*Ty+k*Tx+1) && (n < BS+kk*Tx*Ty+(k+1)*Tx))
                BigM_i(n,n) = (-2*sigmax_i-2*sigmay_i-2*sigmaz_i)/ht^2;
                BigM_i(n,n-1) = sigmax_i/ht^2;
                BigM_i(n,n+1) = sigmax_i/ht^2;
                BigM_i(n,n-Tx) = sigmay_i/ht^2;
                BigM_i(n,n+Tx) = sigmay_i/ht^2;
                BigM_i(n,n-Tx*Ty) = sigmaz_i/ht^2;
                BigM_i(n,n+Tx*Ty) = sigmaz_i/ht^2;
            end
        end
    end
end
for n = BS+TS:TS+2*BS
    BigM_i(n,n) = 1;
end

% Laplacian matrix for sigma_e in tissue
M_e = spalloc(TS,TS,2*Tx*Ty+2*(Ty-2)*(Tz-2)+6*(Tx-2)*(Ty-2)*(Tz-2));
for n = 1:TS
    M_e(n,n) = 1;
    if n < Tx*Ty+1
        for k = 1:Ty-2
        if n > k*Tx+1 && n < (k+1)*Tx
        M_e(n,n) = (-2*sigmax_i-2*sigmay_i)/ht^2;
        M_e(n,n-1) = sigmax_i/ht^2;
        M_e(n,n+1) = sigmax_i/ht^2;
        M_e(n,n-Tx) = sigmay_i/ht^2;
        M_e(n,n+Tx) = sigmay_i/ht^2;
        end
        end
    end
    for kk = 1:Tz-2
        for k = 1:Ty-2
            if ((n > kk*Tx*Ty+k*Tx+1) && (n < kk*Tx*Ty+(k+1)*Tx))
                M_e(n,n) = (-2*sigmax_e-2*sigmay_e-2*sigmaz_e)/ht^2;
                M_e(n,n-1) = sigmax_e/ht^2;
                M_e(n,n+1) = sigmax_e/ht^2;
                M_e(n,n-Tx) = sigmay_e/ht^2;
                M_e(n,n+Tx) = sigmay_e/ht^2;
                M_e(n,n-Tx*Ty) = sigmaz_e/ht^2;
                M_e(n,n+Tx*Ty) = sigmaz_e/ht^2;
            end
        end
    end
end

% Laplacian Matrix for (sigma_i + sigma_e)in tissue and bath
BigM_ie = spalloc(TS+2*BS,TS+2*BS,2*Tx*Ty+2*(Ty-2)*(Tz-2)+...
    6*(Tx-2)*(Ty-2)*(Tz-2)+2*BS+12*(Bx-2)*(By-2)*(Bz-2));
for n = 1:BS
    BigM_ie(n,n) = 1;
    for kk = 1:Bz-1
        for k = 1:By-2
            if ((n > kk*Bx*By+k*Bx+1) && (n < kk*Bx*By+(k+1)*Bx))
                BigM_ie(n,n) = (-2*sigmax_b-2*sigmay_b-2*sigmaz_b)/hb^2;
                BigM_ie(n,n-1) = sigmax_b/hb^2;
                BigM_ie(n,n+1) = sigmax_b/hb^2;
                BigM_ie(n,n-Bx) = sigmay_b/hb^2;
                BigM_ie(n,n+Bx) = sigmay_b/hb^2;
                BigM_ie(n,n-Bx*By) = sigmaz_b/hb^2;
                BigM_ie(n,n+Bx*By) = sigmaz_b/hb^2;
            end
        end
    end
end
for n = BS+1:BS+TS
    BigM_ie(n,n) = 1;
    if n < BS+Tx*Ty+1
        for k = 1:Ty-2
        if n > BS+k*Tx+1 && n < BS+(k+1)*Tx
        BigM_ie(n,n) = (-(sigmax_e+sigmax_b)-(sigmay_e+sigmay_b)-sigmaz_e-sigmaz_b)/ht^2;
        BigM_ie(n,n-1) = (sigmax_e+sigmax_b)/2*ht^2;
        BigM_ie(n,n+1) = (sigmax_e+sigmax_b)/2*ht^2;
        BigM_ie(n,n-Tx) = (sigmay_e+sigmay_b)/2*ht^2;
        BigM_ie(n,n+Tx) = (sigmay_e+sigmay_b)/2*ht^2;
        BigM_ie(n,n-Tx*Ty) = sigmaz_b/hb^2;
        BigM_ie(n,n+Tx*Ty) = sigmaz_e/ht^2;
        end
        end
    end
    for kk = 1:Tz-2
        for k = 1:Ty-2
            if ((n > BS+kk*Tx*Ty+k*Tx+1) && (n < BS+kk*Tx*Ty+(k+1)*Tx))
                BigM_ie(n,n) = (-2*(sigmax_i+sigmax_e)-2*(sigmay_i+sigmay_e)-2*(sigmaz_i+sigmaz_e))/ht^2;
                BigM_ie(n,n-1) = (sigmax_i+sigmax_e)/ht^2;
                BigM_ie(n,n+1) = (sigmax_i+sigmax_e)/ht^2;
```

```
                BigM_ie(n,n-Tx) = (sigmay_i+sigmay_e)/ht^2;
                BigM_ie(n,n+Tx) = (sigmay_i+sigmay_e)/ht^2;
                BigM_ie(n,n-Tx*Ty) = (sigmaz_i+sigmaz_e)/ht^2;
                BigM_ie(n,n+Tx*Ty) = (sigmaz_i+sigmaz_e)/ht^2;
            end
        end
    end
    if n > BS+Tx*Ty*(Tz-1)
        BigM_ie(n,n) = (-(sigmax_e+sigmax_b)-(sigmay_e+sigmay_b)-sigmaz_e-sigmaz_b)/ht^2;
        BigM_ie(n,n-1) = (sigmax_e+sigmax_b)/2*ht^2;
        BigM_ie(n,n+1) = (sigmax_e+sigmax_b)/2*ht^2;
        BigM_ie(n,n-Tx) = (sigmay_e+sigmay_b)/2*ht^2;
        BigM_ie(n,n+Tx) = (sigmay_e+sigmay_b)/2*ht^2;
        BigM_ie(n,n-Tx*Ty) = sigmaz_e/ht^2;
        BigM_ie(n,n+Tx*Ty) = sigmaz_b/hb^2;
    end
end
for n = BS+TS+1:TS+2*BS
    BigM_ie(n,n) = 1;
    for kk = 1:Bz-1
        for k = 1:By-2
            if ((n > BS+TS+(kk-1)*Bx*By+k*Bx+1) && (n < BS+TS+(kk-1)*Bx*By+(k+1)*Bx))
                BigM_ie(n,n) = (-2*sigmax_b-2*sigmay_b-2*sigmaz_b)/hb^2;
                BigM_ie(n,n-1) = sigmax_b/hb^2;
                BigM_ie(n,n+1) = sigmax_b/hb^2;
                BigM_ie(n,n-Bx) = sigmay_b/hb^2;
                BigM_ie(n,n+Bx) = sigmay_b/hb^2;
                BigM_ie(n,n-Bx*By) = sigmaz_b/hb^2;
                BigM_ie(n,n+Bx*By) = sigmaz_b/hb^2;
            end
        end
    end
end

neg_BigM_ie = -BigM_ie; % makes bicstabl applicable (positive definiteness)

%% Parameters from the Ten Tusscher model
% Electrophysiological parameters
Ko  = ones(TS,1)*5.4;   % Extracellular K concentration [mM]
Cao = ones(TS,1)*2.0;   % Extracellualr Ca concentration [mM]
Nao = ones(TS,1)*140.0; % Extracellular Na concentration [mM]

Vc  = ones(TS,1)*0.016404;      % Volume of the cytoplasm [mm^3]
Vsr = ones(TS,1)*0.001094;      % Volum of sarcoplasmatic reticulum [mm^3]
Vss = ones(TS,1)*0.00005468;    % Volume of the subspace [mm^3]

Capacitance = ones(TS,1)*0.185; % Cellular capacitance [nF]

Bufc   = ones(TS,1)*0.2;    % Cytoplasmic Ca buffer concentration [mM]
Kbufc  = ones(TS,1)*0.001;  % Cai, half-saturation constant for cytopl. buffer [mM]
Bufsr  = ones(TS,1)*10.0;   % Sarcoplasmic Ca buffer concentration [mM]
Kbufsr = ones(TS,1)*0.3;    % CaSR half-saturation constant for SR buffer [mM]
Bufss  = ones(TS,1)*0.4;    % Subspace Ca buffer concentration [mM]
Kbufss = ones(TS,1)*0.00025;% CaSS half-saturation constant for SS buffer [mM]

Vmaxup = ones(TS,1)*0.006375;   % Maximal Iup conductance [mM/ms]
Kup    = ones(TS,1)*0.00025;    % Half-saturation constant of Iup [mM]

Vrel   = ones(TS,1)*0.102;   % Maximal Irel conductance [mM/ms]
k1_    = ones(TS,1)*0.15;    % Irel transition rate R to O and RI to I [1/mM^2*ms]
k2_    = ones(TS,1)*0.045;   % Irel transition rate O to I and R to RI [1/mM*ms]
k3     = ones(TS,1)*0.06;    % Irel transition rate O to R and I to RI [1/ms]
k4     = ones(TS,1)*0.005;   % Irel transition rate I to O and RI to I [1/ms]

EC     = ones(TS,1)*1.5;    % CaSR half-saturation constant of kCaSR [mM]
maxsr  = ones(TS,1)*2.5;    % Maximum value of kCaSR (dimensionless)
minsr  = ones(TS,1);        % Minimum value of kCaSR (dimensionless)

Vleak  = ones(TS,1)*0.00036;    % Maximal Ileak conductance [mM/ms]
Vxfer  = ones(TS,1)*0.0038;     % Maximal Ixfer conductance [mM/ms]

R = 8314.472;       % Gas constant [mJ/K*mol]
F = 96485.3415;     % Faraday constant [C/mol]
T = 310;            % Temperature [K]
RTonF = ones(TS,1)*(R*T/F);

% Parameters for ion currents
GKr = ones(TS,1)*0.153;     % Maximal IKr conductance [nS/pF]
GKs = ones(TS,1)*0.392;     % Maximal IKs conductance [nS/pF]
GKs(1:endo) = 0.392;        % Maximal IKs conductance endocard [nS/pF]
GKs(endo+1:myo) = 0.098;    % Maximal IKs conductance midmyocard [nS/pF]
GKs(myo+1:epi) = 0.329;     % Maximal IKs conductance epicard [nS/pF]
GK1 = ones(TS,1)*5.405;     % Maximal IK1 conductance [nS/pF]
Gto = ones(TS,1)*0.294;     % Maximal Ito conductance [nS/pF]
Gto(1:endo) = 0.073;        % Maximal Ito conductance endocard [nS/pF]
Gto(endo+1:myo) = 0.294;    % Maximal Ito conductance midmyocard [nS/pF]
Gto(myo+1:epi) = 0.294;     % Maximal Ito conductance epicard [nS/pF]
GNa    = ones(TS,1)*14.838;  % Maximal INa conductance [nS/pF]
GbNa   = ones(TS,1)*0.00029; % Maximal background-INa conductance [nS/pF]
```

```
KmK   = ones(TS,1);
KmNa  = ones(TS,1)*40.0;
knak  = ones(TS,1)*2.724;
pKNa  = ones(TS,1)*0.03;
GCaL  = ones(TS,1)*0.0000398;
GbCa  = ones(TS,1)*0.000592;
knaca = ones(TS,1)*1000;
KmNai = ones(TS,1)*87.5;
KmCa  = ones(TS,1)*1.38;
ksat  = ones(TS,1)*0.1;
n     = ones(TS,1)*0.35;     % Voltage dependence parameter of INaCa
GpCa  = ones(TS,1)*0.1238;
KpCa  = ones(TS,1)*0.0005;
GpK   = ones(TS,1)*0.0146;

% Initial conditions  for state variables
inverseVcF   = 1./(Vc*F);
inverseVcF2  = inverseVcF./2;
inverseVssF2 = 1./(2*Vss*F);
svolt  = ones(TS,1)*-86.2;
Cai    = ones(TS,1)*0.00007;
CaSR   = ones(TS,1)*1.3;
CaSS   = ones(TS,1)*0.0007;
Nai    = ones(TS,1)*7.67;
Ki     = ones(TS,1)*138.3;
sm     = zeros(TS,1);
sh     = ones(TS,1)*0.75;
sj     = ones(TS,1)*0.75;
sxr1   = zeros(TS,1);
sxr2   = ones(TS,1);
sxs    = zeros(TS,1);
sr     = zeros(TS,1);
ss     = ones(TS,1);
sd     = zeros(TS,1);
sf     = ones(TS,1);
sf2    = ones(TS,1);
sfcass = ones(TS,1);
sRR    = ones(TS,1);
sOO    = zeros(TS,1);
% End of Electrophysiological parameters

%% MODEL
Vm = ones(TS,N)*-86.2e-3;
Vhelp = zeros(TS+2*BS,1);   % V for calculating phi_e in bath and tissue
Vhelp(BS+1:BS+TS) = Vm(:,1);
phi_e = zeros(TS,N);
Big_phi = zeros(TS+2*BS,1);
neg_Big_phi = -Big_phi;


for i = 1:N-1

    % TEN TUSSCHER PART
    VmTT = Vm(:,i)*1000; % TT requires Vm in [mV] -> helping variable

    % Parameters needed to calculate ion currents
    EK  = RTonF .* log(Ko./Ki);
    ENa = RTonF .* log(Nao./Nai);
    EKs = RTonF .* log((Ko+pKNa.*Nao)./(Ki+pKNa.*Nai));
    ECa = 0.5*RTonF.*log(Cao./Cai);
    AK1 = 0.1./(1+exp(0.06*(VmTT-EK-200)));
    BK1 = (3*exp(0.0002*(VmTT-EK+100)) + exp(0.1*(VmTT-EK-10))) ./ ...
        (1+exp(-0.5*(VmTT-EK)));
    rec_iK1  = AK1./(AK1+BK1);
    rec_iNaK = 1 ./ ...
        (1+0.1245*exp(-0.1*VmTT./RTonF)+0.0353*exp(-VmTT./RTonF));
    rec_ipK = 1 ./ (1+exp((25-VmTT)./5.98));

    % Calculate ion currents
    INa  = GNa.*(sm.^3).*sh.*sj.*(VmTT-ENa);
    svolt_etc = 2*(VmTT-15)./RTonF;
    ICaL = GCaL.*sd.*sf.*sf2.*sfcass.*2.*F.*svolt_etc .* ...
        (0.25.*exp(svolt_etc).*CaSS-Cao) ./ (exp(svolt_etc)-1);
    Ito = Gto.*sr.*ss.*(VmTT-EK);
    IKr = GKr.*sqrt(Ko/5.4).*sxr1.*sxr2.*(VmTT-EK);
    IKs = GKs.*sxs.*sxs.*(VmTT-EKs);
    IK1 = GK1.*rec_iK1.*(VmTT-EK);
    INaCa = knaca.*(1./((KmNai.^3)+(Nao.^3))).*(1./(KmCa+Cao)).* ...
        (1./(1+ksat.*exp((n-1).* VmTT./RTonF))).* ...
        (exp(n.*VmTT./RTonF).*(Nai.^3).*Cao-exp((n-1).*VmTT./RTonF).* ...
        (Nao.^3).*Cai*2.5);
    INaK = knak.*(Ko./(Ko+KmK)).*(Nai./(Nai+KmNa)).*rec_iNaK;
    IpCa = GpCa.*Cai./(KpCa+Cai);
    IpK  = GpK.*rec_ipK.*(VmTT-EK);
    IbNa = GbNa.*(VmTT-ENa);
    IbCa = GbCa.*(VmTT-ECa);
    Iion = IKr+IKs+IK1+Ito+INa+IbNa+ICaL+IbCa+INaK+INaCa+IpCa+IpK;

    % Update concentrations
```

```
    kCaSR = maxsr-(maxsr-minsr)./(1+(EC./CaSR).^2);
    k1    = k1_./kCaSR;
    k2    = k2_.*kCaSR;
    dRR   = k4.*(1-sRR)-k2.*CaSS.*sRR;
    sRR   = sRR+delta_t*dRR;
    sOO   = k1.*CaSS.*CaSS.*sRR./(k3+k1.*CaSS.*CaSS);
    Irel  = Vrel.*sOO.*(CaSR-CaSS);
    Ileak = Vleak.*(CaSR-Cai);
    Iup   = Vmaxup./(1+(Kup./Cai).^2);
    Ixfer = Vxfer.*(CaSS-Cai);
    CaCSQN = Bufsr.*CaSR./(CaSR+Kbufsr);
    dCaSR  = delta_t*(Iup-Irel-Ileak);
    bjsr   = Bufsr-CaCSQN-dCaSR-CaSR+Kbufsr;
    cjsr   = Kbufsr.*(CaCSQN+dCaSR+CaSR);
    CaSR   = (sqrt(bjsr.*bjsr+4*cjsr)-bjsr)/2;
    CaSSBuf = Bufss.*CaSS./(CaSS+Kbufss);
    dCaSS   = delta_t.*(-Ixfer.*(Vc./Vss)+Irel.*(Vsr./Vss)+(-ICaL.*inverseVssF2.*...
        Capacitance));
    bcss    = Bufss-CaSSBuf-dCaSS-CaSS+Kbufss;
    ccss    = Kbufss.*(CaSSBuf+dCaSS+CaSS);
    CaSS    = (sqrt(bcss.*bcss+4*ccss)-bcss)./2;
    CaBuf = Bufc.*Cai./(Kbufc+Cai);
    dCai  = delta_t.*((-(IbCa+IpCa-2*INaCa).*inverseVcF2.*Capacitance)- ...
        (Iup-Ileak).*(Vsr./Vc)+Ixfer);
    bc    = Bufc-CaBuf-dCai-Cai+Kbufc;
    cc    = Kbufc.*(CaBuf+dCai+Cai);
    Cai   = (sqrt(bc.*bc+4*cc)-bc)./2;
    dNai = -(INa+IbNa+3*INaK+3*INaCa).*inverseVcF.*Capacitance;
    Nai  = Nai + delta_t*dNai;
    dKi = -(IK1+Ito+IKr+IKs-2*INaK+IpK).*inverseVcF.*Capacitance;
    Ki  = Ki + delta_t*dKi;

    % Calculate steady state values and time constants (gating parameters)
    AM    = 1./(1+exp((-60-VmTT)/5));
    BM    = 0.1./(1+exp((VmTT+35)/5))+0.1./(1+exp((VmTT-50)/200));
    Tau_M = AM.*BM;
    M_Inf = 1./((1+exp((-56.86-VmTT)/9.03)).^2);

    for k = 1:TS
        if VmTT(k)>-40
            AH(k,1)  = 0;
            BH(k,1)  = 0.77./(0.13*(1+exp(-(VmTT(k)+10.66)/11.1)));
        else
            AH(k,1)  = (0.057*exp(-(VmTT(k)+80)/6.8));
            BH(k,1)  = 2.7*exp(0.079*VmTT(k))+3.1e5*exp(0.3485*VmTT(k));
        end
        if VmTT(k)>-40
            AJ(k,1)  = 0;
            BJ(k,1)  = (0.6*exp((0.057)*VmTT(k))./(1+exp(-0.1*(VmTT(k)+32))));
        else
            AJ(k,1)  = (((-2.5428e4).*exp(0.2444.*VmTT(k))-(6.948e-6).* ...
                exp(-0.04391.*VmTT(k))).*(VmTT(k)+37.78)./ ...
                (1+exp(0.311.*(VmTT(k)+79.23))));
            BJ(k,1)  = (0.02424.*exp(-0.01052.*VmTT(k))./ ...
                (1+exp(-0.1378.*(VmTT(k)+40.14))));
        end
    end
    Tau_H = 1./(AH+BH);
    Tau_J = 1./(AJ+BJ);
    H_Inf = 1./((1+exp(VmTT+71.55)/7.43)).^2;
    J_Inf = H_Inf;

    Xr1_Inf = 1./(1+exp((-26-VmTT)/7));
    axr1    = 450./(1+exp((-45-VmTT)/10));
    bxr1    = 6./(1+exp((VmTT+30)/11.5));
    Tau_Xr1 = axr1.*bxr1;

    Xr2_Inf = 1./(1+exp((VmTT+88)/24));
    axr2    = 3./(1+exp((-60-VmTT)/20));
    bxr2    = 1.12./(1+exp((VmTT-60)/20));
    Tau_Xr2 = axr2.*bxr2;

    Xs_Inf  = 1./(1+exp((-5-VmTT)/14));
    Axs     = 1400./(sqrt(1+exp((5-VmTT)/6)));
    Bxs     = 1./(1+exp((VmTT-35)/15));
    Tau_Xs  = Axs.*Bxs+80;

    R_Inf = 1./(1+exp((20-VmTT)/6));
    Tau_R = 9.5*exp(-((VmTT+40).^2)/1800)+0.8;
    S_Inf(1:endo,1) = 1./(1+exp((VmTT(1:endo)+28)/5));
    S_Inf(endo+1:myo,1) = 1./(1+exp((VmTT(endo+1:myo)+20)/5));
    S_Inf(myo+1:epi,1) = 1./(1+exp((VmTT(myo+1:epi)+20)/5));
    Tau_S(1:endo,1) = 1000*exp(-((VmTT(1:endo)+67).^2)./1000)+8;
    Tau_S(endo+1:myo,1) = 85*exp(-((VmTT(endo+1:myo)+45).^2)/320)+...
        5./(1+exp((VmTT(endo+1:myo)-20)/5))+3;
    Tau_S(myo+1:epi,1) = 85*exp(-((VmTT(myo+1:epi)+45).^2)/320)+...
        5./(1+exp((VmTT(myo+1:epi)-20)/5))+3;

    D_Inf = 1./(1+exp((-8-VmTT)/7.5));
```

```
    Ad    = 1.4./(1+exp((-35-VmTT)/13))+0.25;
    Bd    = 1.4./(1+exp((VmTT+5)/5));
    Cd    = 1./(1+exp((50-VmTT)/20));
    Tau_D = Ad.*Bd.*Cd;

    F_Inf = 1./(1+exp((VmTT+20)/7));
    Af    = 1102.5*exp(-((VmTT+27).^2)/225);
    Bf    = 200./(1+exp((13-VmTT)/10));
    Cf    = (180./(1+exp((VmTT+30)/10)))+20;
    Tau_F = Af+Bf+Cf;

    F2_Inf = 0.67./(1+exp((VmTT+35)/7))+0.33;
    Af2    = 600*exp(-((VmTT+25).^2)/170);
    Bf2    = 31./(1+exp((25-VmTT)/10));
    Cf2    = 16./(1+exp((VmTT+30)/10));
    Tau_F2 = Af2+Bf2+Cf2;
    FCaSS_Inf = 0.6./(1+400*CaSS.*CaSS)+0.4;
    Tau_FCaSS = 80./(1+400*CaSS.*CaSS)+2;

    % Update gates
    sm     = M_Inf-(M_Inf-sm).*exp(-delta_t./Tau_M);
    sh     = H_Inf-(H_Inf-sh).*exp(-delta_t./Tau_H);
    sj     = J_Inf-(J_Inf-sj).*exp(-delta_t./Tau_J);
    sxr1   = Xr1_Inf-(Xr1_Inf-sxr1).*exp(-delta_t./Tau_Xr1);
    sxr2   = Xr2_Inf-(Xr2_Inf-sxr2).*exp(-delta_t./Tau_Xr2);
    sxs    = Xs_Inf-(Xs_Inf-sxs).*exp(-delta_t./Tau_Xs);
    ss     = S_Inf-(S_Inf-ss).*exp(-delta_t./Tau_S);
    sr     = R_Inf-(R_Inf-sr).*exp(-delta_t./Tau_R);
    sd     = D_Inf-(D_Inf-sd).*exp(-delta_t./Tau_D);
    sf     = F_Inf-(F_Inf-sf).*exp(-delta_t./Tau_F);
    sf2    = F2_Inf-(F2_Inf-sf2).*exp(-delta_t./Tau_F2);
    sfcass = FCaSS_Inf-(FCaSS_Inf-sfcass).*exp(-delta_t./Tau_FCaSS);

    %  BIDOMAIN PART
    neg_Big_phi(:,i) = bicgstabl(neg_BigM_ie,(BigM_i*Vhelp));
    Big_phi(:,i) = -neg_Big_phi(:,i);
    phi_e(:,i) = Big_phi(BS+1:BS+TS,i);

    if i <= t_stim
%         dVmdt = (-*M_e*phi_e(:,i)+ Istim)/((beta*Cm)/1000)-(Iion*2e-2)/Cm;
        dVmdt = (-0*M_e*phi_e(:,i)+ Istim)/((beta*Cm)/1000)-(Iion*2e-2)/Cm;
    else
%         dVmdt = (-*M_e*phi_e(:,i))/(beta*Cm)-(Iion*2e-2)/Cm;
        dVmdt = (-0*M_e*phi_e(:,i))/(beta*Cm)-(Iion*2e-2)/Cm;
    end

    for kz = 1:Tz
        dVmdt((kz-1)*Tx*Ty+1:(kz-1)*Tx*Ty+Tx+1,1) = 0;
        dVmdt((kz-1)*Tx*Ty+(Ty-1)*Tx:(kz-1)*Tx*Ty+Tx*Ty,1) = 0;
        for ky = 2:Ty-2
            dVmdt((kz-1)*Tx*Ty+ky*Tx:(kz-1)*Tx*Ty+ky*Tx+1,1) = 0;
        end
    end

    Vm(:,i+1) = Vm(:,i)+dVmdt*(delta_t/1000);
    Vhelp(BS+1:BS+TS) = Vm(:,i+1);

    disp(i);
end
```

Appendix B

Full MATLAB code of the monodomain model with incorporated Ten Tusscher model.

```
%% ACTIVE MONODOMAIN 3D - Versuch
% Run und dann folgendes plotten:
% figure;plot((0:N-1)*delta_t,Vm(P,:));
% hold on;plot((0:N-1)*delta_t,Vm(P+1,:));
% hold on;plot((0:N-1)*delta_t,Vm(P+2,:));
% hold on;plot((0:N-1)*delta_t,Vm(P+3,:));

clc
%clear all; %close all;

%% Tissue Grid
Lx = 50;     % grid length in x direction
Ly = 50;     % grid length in y direction
Lz = 20;     % grid length in z direction
h = 0.2e-3;  % distance between grid points [m]

%% Time steps
delta_t = 0.02; % size of time step [ms]
N = 1000;       % number of time steps

%% Stimulus
Stimulus = 500;     % stimulus current[A/m^2] 200 without coupling
t_stim_on = 5;      % sart of stimulus [ms]
t_stim = 1;         % stimulus duration [ms]
t_stim_on =t_stim_on/delta_t;
t_stim = t_stim/delta_t;

x = 30;        % x position of stimulus point
y = 30;        % y position of stimulus point
z = 15;        % z position of stimulus point

P = x+(y-1)*Lx+(z-1)*Lx*Ly;     % calculation of point number
Istim = zeros(Lx*Ly*Lz,1);
Istim(P,1) = Stimulus;

%% Membrane parameters
Cm = 1e-2;      % 3e-2 capacitance [F/m^2]
beta = 3e5;     % surface to volume ratio [1/m]

% Conductivity
sigmax_i = 0.2;     % intracell. along fibre (x dir.) [S/m]
sigmay_i = 0.02;    % intracell. vertical to fibre (y dir.) [S/m]
sigmaz_i = 0.02;    % intracell. vertical to fibre (z dir.) [S/m]
sigmax_e = 0.2;     % extracell. along fibre (x dir.) [S/m]
sigmay_e = 0.08;    % extracell. vertical to fibre (y dir.) [S/m]
sigmaz_e = 0.08;    % extracell. vertical to fibre (z dir.) [S/m]

%intracellular
M_i = spalloc(Lx*Ly*Lz,Lx*Ly*Lz,2*Lx*Ly+2*(Ly-2)*(Lz-2)+6*(Lx-2)*(Ly-2)*(Lz-2));
for n = 1:(Lx*Ly*Lz)
    M_i(n,n) = 1;
    for kk = 1:Lz-2
        for k = 1:Ly-2
            if ((n > kk*Lx*Ly+k*Lx+1) && (n < kk*Lx*Ly+(k+1)*Lx))
                M_i(n,n) = (-2*sigmax_i-2*sigmay_i-2*sigmaz_i)/h^2;
                M_i(n,n-1) = sigmax_i/h^2;
                M_i(n,n+1) = sigmax_i/h^2;
                M_i(n,n-Lx) = sigmay_i/h^2;
                M_i(n,n+Lx) = sigmay_i/h^2;
                M_i(n,n-Lx*Ly) = sigmaz_i/h^2;
                M_i(n,n+Lx*Ly) = sigmaz_i/h^2;
            end
        end
    end
end

%extracellular
M_e = spalloc(Lx*Ly*Lz,Lx*Ly*Lz,2*Lx*Ly+2*(Ly-2)*(Lz-2)+6*(Lx-2)*(Ly-2)*(Lz-2));
for n = 1:(Lx*Ly*Lz)
    M_e(n,n) = 1;
    for kk = 1:Lz-2
        for k = 1:Ly-2
            if ((n > kk*Lx*Ly+k*Lx+1) && (n < kk*Lx*Ly+(k+1)*Lx))
                M_e(n,n) = (-2*sigmax_e-2*sigmay_e-2*sigmaz_e)/h^2;
                M_e(n,n-1) = sigmax_e/h^2;
                M_e(n,n+1) = sigmax_e/h^2;
                M_e(n,n-Lx) = sigmay_e/h^2;
                M_e(n,n+Lx) = sigmay_e/h^2;
                M_e(n,n-Lx*Ly) = sigmaz_e/h^2;
                M_e(n,n+Lx*Ly) = sigmaz_e/h^2;
            end
        end
```

```
    end
end

%intra+extracellular
M_ie = spalloc(Lx*Ly*Lz,Lx*Ly*Lz,2*Lx*Ly+2*(Ly-2)*(Lz-2)+6*(Lx-2)*(Ly-2)*(Lz-2));
for n = 1:(Lx*Ly*Lz)
    M_ie(n,n) = 1;
    for kk = 1:Lz-2
        for k = 1:Ly-2
            if ((n > kk*Lx*Ly+k*Lx+1) && (n < kk*Lx*Ly+(k+1)*Lx))
                M_ie(n,n) = (-2*(sigmax_i+sigmax_e)-2*(sigmay_i+sigmay_e)-2*(sigmaz_i+sigmaz_e))/h^2;
                M_ie(n,n-1) = (sigmax_i+sigmax_e)/h^2;
                M_ie(n,n+1) = (sigmax_i+sigmax_e)/h^2;
                M_ie(n,n-Lx) = (sigmay_i+sigmay_e)/h^2;
                M_ie(n,n+Lx) = (sigmay_i+sigmay_e)/h^2;
                M_ie(n,n-Lx*Ly) = (sigmaz_i+sigmaz_e)/h^2;
                M_ie(n,n+Lx*Ly) = (sigmaz_i+sigmaz_e)/h^2;
            end
        end
    end
end

%% Parameters TT
% Electrophysiological parameters
Ko  = ones(Lx*Ly*Lz,1)*5.4;     % Extracellular K concentration [mM]
Cao = ones(Lx*Ly*Lz,1)*2.0;     % Extracellualr Ca concentration [mM]
Nao = ones(Lx*Ly*Lz,1)*140.0;   % Extracellular Na concentration [mM]

Vc  = ones(Lx*Ly*Lz,1)*0.016404;   % Volume of the cytoplasm [mm^3]
Vsr = ones(Lx*Ly*Lz,1)*0.001094;   % Volum of sarcoplasmatic reticulum [mm^3]
Vss = ones(Lx*Ly*Lz,1)*0.00005468; % Volume of the subspace [mm^3]

Capacitance = ones(Lx*Ly*Lz,1)*0.185; % Cellular capacitance [nF]

Bufc   = ones(Lx*Ly*Lz,1)*0.2;     % Cytoplasmic Ca buffer concentration [mM]
Kbufc  = ones(Lx*Ly*Lz,1)*0.001;   % Cai, half-saturation constant for cytopl. buffer [mM]
Bufsr  = ones(Lx*Ly*Lz,1)*10.0;    % Sarcoplasmic Ca buffer concentration [mM]
Kbufsr = ones(Lx*Ly*Lz,1)*0.3;     % CaSR half-saturation constant for SR buffer (mM)
Bufss  = ones(Lx*Ly*Lz,1)*0.4;     % Subspace Ca buffer concentration [mM]
Kbufss = ones(Lx*Ly*Lz,1)*0.00025; % CaSS half-saturation constant for SS buffer [mM]

Vmaxup = ones(Lx*Ly*Lz,1)*0.006375;% Maximal Iup conductance [mM/ms]
Kup    = ones(Lx*Ly*Lz,1)*0.00025; % Half-saturation constant of Iup [mM]

Vrel   = ones(Lx*Ly*Lz,1)*0.102;   % Maximal Irel conductance [mM/ms]
k1_    = ones(Lx*Ly*Lz,1)*0.15;    % Irel transition rate R to O and RI to I [1/mM^2*ms]
k2_    = ones(Lx*Ly*Lz,1)*0.045;   % Irel transition rate O to I and R to RI [1/mM*ms]
k3     = ones(Lx*Ly*Lz,1)*0.06;    % Irel transition rate O to R and I to RI [1/ms]
k4     = ones(Lx*Ly*Lz,1)*0.005;   % Irel transition rate I to O and RI to I [1/ms]

EC     = ones(Lx*Ly*Lz,1)*1.5;     % CaSR half-saturation constant of kCaSR [mM]
maxsr  = ones(Lx*Ly*Lz,1)*2.5;     % Maximum value of kCaSR (dimensionless)
minsr  = ones(Lx*Ly*Lz,1);     % Minimum value of kCaSR (dimensionless)

Vleak  = ones(Lx*Ly*Lz,1)*0.00036; % Maximal Ileak conductance [mM/ms]
Vxfer  = ones(Lx*Ly*Lz,1)*0.0038;  % Maximal Ixfer conductance [mM/ms]

R = 8314.472;     % Gas constant [mJ/K*mol]
F = 96485.3415;   % Faraday constant [C/mol]
T = 310;          % Temperature [K]
RTonF = ones(Lx*Ly*Lz,1)*(R*T/F);

% Parameters for ion currents
GKr = ones(Lx*Ly*Lz,1)*0.153;       % Maximal IKr conductance [nS/pF]
GKs = ones(Lx*Ly*Lz,1)*0.392;       % Maximal IKs conductance [nS/pF]
GK1 = ones(Lx*Ly*Lz,1)*5.405;       % Maximal IK1 conductance [nS/pF]
Gto = ones(Lx*Ly*Lz,1)*0.294;       % Maximal Ito conductance [nS/pF]
GNa   = ones(Lx*Ly*Lz,1)*14.838;    % Maximal INa conductance [nS/pF]
GbNa  = ones(Lx*Ly*Lz,1)*0.00029;   % Maximal background-INa conductance [nS/pF]
KmK   = ones(Lx*Ly*Lz,1);
KmNa  = ones(Lx*Ly*Lz,1)*40.0;
knak  = ones(Lx*Ly*Lz,1)*2.724;
pKNa  = ones(Lx*Ly*Lz,1)*0.03;
GCaL  = ones(Lx*Ly*Lz,1)*0.0000398;
GbCa  = ones(Lx*Ly*Lz,1)*0.000592;
knaca = ones(Lx*Ly*Lz,1)*1000;
KmNai = ones(Lx*Ly*Lz,1)*87.5;
KmCa  = ones(Lx*Ly*Lz,1)*1.38;
ksat  = ones(Lx*Ly*Lz,1)*0.1;
n     = ones(Lx*Ly*Lz,1)*0.35;       % Voltage dependence parameter of INaCa
GpCa  = ones(Lx*Ly*Lz,1)*0.1238;
KpCa  = ones(Lx*Ly*Lz,1)*0.0005;
GpK   = ones(Lx*Ly*Lz,1)*0.0146;

% Initial conditions  for state variables
inverseVcF   = 1./(Vc*F);
inverseVcF2  = inverseVcF./2;
inverseVssF2 = 1./(2*Vss*F);
```

```
svolt  = ones(Lx*Ly*Lz,1)*-86.2;
Cai    = ones(Lx*Ly*Lz,1)*0.00007;
CaSR   = ones(Lx*Ly*Lz,1)*1.3;
CaSS   = ones(Lx*Ly*Lz,1)*0.0007;
Nai    = ones(Lx*Ly*Lz,1)*7.67;
Ki     = ones(Lx*Ly*Lz,1)*138.3;
sm     = zeros(Lx*Ly*Lz,1);
sh     = ones(Lx*Ly*Lz,1)*0.75;
sj     = ones(Lx*Ly*Lz,1)*0.75;
sxr1   = zeros(Lx*Ly*Lz,1);
sxr2   = ones(Lx*Ly*Lz,1);
sxs    = zeros(Lx*Ly*Lz,1);
sr     = zeros(Lx*Ly*Lz,1);
ss     = ones(Lx*Ly*Lz,1);
sd     = zeros(Lx*Ly*Lz,1);
sf     = ones(Lx*Ly*Lz,1);
sf2    = ones(Lx*Ly*Lz,1);
sfcass = ones(Lx*Ly*Lz,1);
sRR    = ones(Lx*Ly*Lz,1);
sOO    = zeros(Lx*Ly*Lz,1);
% End of Electrophysiological parameters

%% Model
Vm = ones(Lx*Ly*Lz,N)*-86.2e-3;
%phi_e = zeros(Lx*Ly*Lz);


for i = 1:N-1

    VmTT = Vm(:,i)*1000;

    % Parameters needed to calculate ion currents
    EK  = RTonF .* log(Ko./Ki);
    ENa = RTonF .* log(Nao./Nai);
    EKs = RTonF .* log((Ko+pKNa.*Nao)./(Ki+pKNa.*Nai));
    ECa = 0.5*RTonF.*log(Cao./Cai);
    AK1 = 0.1./(1+exp(0.06*(VmTT-EK-200)));
    BK1 = (3*exp(0.0002*(VmTT-EK+100)) + exp(0.1*(VmTT-EK-10))) ./ ...
        (1+exp(-0.5*(VmTT-EK)));
    rec_iK1  = AK1./(AK1+BK1);
    rec_iNaK = 1 ./ ...
        (1+0.1245*exp(-0.1*VmTT./RTonF)+0.0353*exp(-VmTT./RTonF));
    rec_ipK = 1 ./ (1+exp((25-VmTT)./5.98));

    % Calculate ion currents
    INa  = GNa.*(sm.^3).*sh.*sj.*(VmTT-ENa);
    svolt_etc = 2*(VmTT-15)./RTonF;
    ICaL = GCaL.*sd.*sf.*sf2.*sfcass.*2.*F.*svolt_etc .* ...
        (0.25.*exp(svolt_etc).*CaSS-Cao) ./ (exp(svolt_etc)-1);
    Ito = Gto.*sr.*ss.*(VmTT-EK);
    IKr = GKr.*sqrt(Ko/5.4).*sxr1.*sxr2.*(VmTT-EK);
    IKs = GKs.*sxs.*sxs.*(VmTT-EKs);
    IK1 = GK1.*rec_iK1.*(VmTT-EK);
    INaCa = knaca.*(1./((KmNai.^3)+(Nao.^3))).*(1./(KmCa+Cao)).* ...
        (1./(1+ksat.*exp((n-1).* VmTT./RTonF))).* ...
        (exp(n.*VmTT./RTonF).*(Nai.^3).*Cao-exp((n-1).*VmTT./RTonF).* ...
        (Nao.^3).*Cai.*2.5);
    INaK = knak.*(Ko./(Ko+KmK)).*(Nai./(Nai+KmNa)).*rec_iNaK;
    IpCa = GpCa.*Cai./(KpCa+Cai);
    IpK  = GpK.*rec_ipK.*(VmTT-EK);
    IbNa = GbNa.*(VmTT-ENa);
    IbCa = GbCa.*(VmTT-ECa);
    Iion = ((IKr+IKs+IK1+Ito+INa+IbNa+ICaL+IbCa+INaK+INaCa+IpCa+IpK));

    % Update concentrations
    kCaSR = maxsr-(maxsr-minsr)./(1+(EC./CaSR).^2);
    k1    = k1_./kCaSR;
    k2    = k2_.*kCaSR;
    dRR   = k4.*(1-sRR)-k2.*CaSS.*sRR;
    sRR   = sRR+delta_t*dRR;
    sOO   = k1.*CaSS.*CaSS.*sRR./(k3+k1.*CaSS.*CaSS);
    Irel  = Vrel.*sOO.*(CaSR-CaSS);
    Ileak = Vleak.*(CaSR-Cai);
    Iup   = Vmaxup./(1+(Kup./Cai).^2);
    Ixfer = Vxfer.*(CaSS-Cai);
    CaCSQN = Bufsr.*CaSR./(CaSR+Kbufsr);
    dCaSR  = delta_t*(Iup-Irel-Ileak);
    bjsr   = Bufsr-CaCSQN-dCaSR-CaSR+Kbufsr;
    cjsr   = Kbufsr.*(CaCSQN+dCaSR+CaSR);
    CaSR   = (sqrt(bjsr.*bjsr+4*cjsr)-bjsr)/2;
    CaSSBuf = Bufss.*CaSS./(CaSS+Kbufss);
    dCaSS   = delta_t.*(-Ixfer.*(Vc./Vss)+Irel.*(Vsr./Vss)+(-ICaL.*inverseVssF2.*...
        Capacitance));
    bcss    = Bufss-CaSSBuf-dCaSS-CaSS+Kbufss;
    ccss    = Kbufss.*(CaSSBuf+dCaSS+CaSS);
    CaSS    = (sqrt(bcss.*bcss+4*ccss)-bcss)./2;
    CaBuf = Bufc.*Cai./(Kbufc+Cai);
    dCai  = delta_t.*((-(IbCa+IpCa-2*INaCa).*inverseVcF2.*Capacitance)- ...
        (Iup-Ileak).*(Vsr./Vc)+Ixfer);
```

```
    bc    = Bufc-CaBuf-dCai-Cai+Kbufc;
    cc    = Kbufc.*(CaBuf+dCai+Cai);
    Cai   = (sqrt(bc.*bc+4*cc)-bc)./2;
    dNai = -(INa+IbNa+3*INaK+3*INaCa).*inverseVcF.*Capacitance;
    Nai  = Nai + delta_t*dNai;
    %if i<=t_stim
    %   dKi = -(Istim/2e-2+IK1+Ito+IKr+IKs-2*INaK+IpK).*inverseVcF.*Capacitance; %DELETED ISTIM HERE
    %else
    dKi = -(IK1+Ito+IKr+IKs-2*INaK+IpK).*inverseVcF.*Capacitance;
    % end
    Ki  = Ki + delta_t*dKi;
    % Calculate steady state values and time constants (gating parameters)
    AM    = 1./(1+exp((-60-VmTT)/5));
    BM    = 0.1./(1+exp((VmTT+35)/5))+0.1./(1+exp((VmTT-50)/200));
    Tau_M = AM.*BM;
    M_Inf = 1./((1+exp((-56.86-VmTT)/9.03)).^2);
    for k = 1:Lx*Ly*Lz
        if VmTT(k)>-40
            AH(k,1)  = 0;
            BH(k,1)  = 0.77./(0.13*(1+exp(-(VmTT(k)+10.66)/11.1)));
        else
            AH(k,1)  = (0.057*exp(-(VmTT(k)+80)/6.8));
            BH(k,1)  = 2.7*exp(0.079*VmTT(k))+3.1e5*exp(0.3485*VmTT(k));
        end
        if VmTT(k)>-40
            AJ(k,1)  = 0;
            BJ(k,1)  = (0.6*exp((0.057)*VmTT(k))./(1+exp(-0.1*(VmTT(k)+32))));
        else
            AJ(k,1)  = (((-2.5428e4).*exp(0.2444.*VmTT(k))-(6.948e-6).* ...
                exp(-0.04391.*VmTT(k))).*(VmTT(k)+37.78)./ ...
                (1+exp(0.311.*(VmTT(k)+79.23))));
            BJ(k,1)  = (0.02424.*exp(-0.01052.*VmTT(k))./ ...
                (1+exp(-0.1378.*(VmTT(k)+40.14))));
        end
    end
    Tau_H = 1./(AH+BH);
    Tau_J = 1./(AJ+BJ);
    H_Inf = 1./((1+exp(VmTT+71.55)/7.43)).^2;
    J_Inf = H_Inf;

    Xr1_Inf = 1./(1+exp((-26-VmTT)/7));
    axr1    = 450./(1+exp((-45-VmTT)/10));
    bxr1    = 6./(1+exp((VmTT+30)/11.5));
    Tau_Xr1 = axr1.*bxr1;

    Xr2_Inf = 1./(1+exp((VmTT+88)/24));
    axr2    = 3./(1+exp((-60-VmTT)/20));
    bxr2    = 1.12./(1+exp((VmTT-60)/20));
    Tau_Xr2 = axr2.*bxr2;

    Xs_Inf  = 1./(1+exp((-5-VmTT)/14));
    Axs     = 1400./(sqrt(1+exp((5-VmTT)/6)));
    Bxs     = 1./(1+exp((VmTT-35)/15));
    Tau_Xs  = Axs.*Bxs+80;

    R_Inf = 1./(1+exp((20-VmTT)/6));
    Tau_R = 9.5*exp(-((VmTT+40).^2)/1800)+0.8;
    S_Inf = 1./(1+exp((VmTT+20)/5));
    Tau_S = 85*exp(-((VmTT+45).^2)/320)+5./(1+exp((VmTT-20)/5))+3;

    D_Inf = 1./(1+exp((-8-VmTT)/7.5));
    Ad    = 1.4./(1+exp((-35-VmTT)/13))+0.25;
    Bd    = 1.4./(1+exp((VmTT+5)/5));
    Cd    = 1./(1+exp((50-VmTT)/20));
    Tau_D = Ad.*Bd.*Cd;

    F_Inf = 1./(1+exp((VmTT+20)/7));
    Af    = 1102.5*exp(-((VmTT+27).^2)/225);
    Bf    = 200./(1+exp((13-VmTT)/10));
    Cf    = (180./(1+exp((VmTT+30)/10)))+20;
    Tau_F = Af+Bf+Cf;

    F2_Inf = 0.67./(1+exp((VmTT+35)/7))+0.33;
    Af2    = 600*exp(-((VmTT+25).^2)/170);
    Bf2    = 31./(1+exp((25-VmTT)/10));
    Cf2    = 16./(1+exp((VmTT+30)/10));
    Tau_F2 = Af2+Bf2+Cf2;
    FCaSS_Inf = 0.6./(1+400*CaSS.*CaSS)+0.4;
    Tau_FCaSS = 80./(1+400*CaSS.*CaSS)+2;

    % Update gates
    sm     = M_Inf-(M_Inf-sm).*exp(-delta_t./Tau_M);
    sh     = H_Inf-(H_Inf-sh).*exp(-delta_t./Tau_H);
    sj     = J_Inf-(J_Inf-sj).*exp(-delta_t./Tau_J);
    sxr1   = Xr1_Inf-(Xr1_Inf-sxr1).*exp(-delta_t./Tau_Xr1);
    sxr2   = Xr2_Inf-(Xr2_Inf-sxr2).*exp(-delta_t./Tau_Xr2);
    sxs    = Xs_Inf-(Xs_Inf-sxs).*exp(-delta_t./Tau_Xs);
    ss     = S_Inf-(S_Inf-ss).*exp(-delta_t./Tau_S);
    sr     = R_Inf-(R_Inf-sr).*exp(-delta_t./Tau_R);
```

```
    sd     = D_Inf-(D_Inf-sd).*exp(-delta_t./Tau_D);
    sf     = F_Inf-(F_Inf-sf).*exp(-delta_t./Tau_F);
    sf2    = F2_Inf-(F2_Inf-sf2).*exp(-delta_t./Tau_F2);
    sfcass = FCaSS_Inf-(FCaSS_Inf-sfcass).*exp(-delta_t./Tau_FCaSS);

    %     mp = -(M_i*Vm(:,i));
    %     phi_e(:,i) = M_ie\mp;
    mv(:,i) = M_i*Vm(:,i);
    for kz = 1:Lz
        mv((kz-1)*Lx*Ly+1:(kz-1)*Lx*Ly+Lx+1,i) = 0;
        mv((kz-1)*Lx*Ly+(Ly-1)*Lx:(kz-1)*Lx*Ly+Lx*Ly,i) = 0;
        for ky = 2:Ly-2
            mv((kz-1)*Lx*Ly+ky*Lx:(kz-1)*Lx*Ly+ky*Lx+1,i) = 0;
        end
    end
    mv(1:Lx*Ly,i)=0;
    mv(Lx*Ly*(Lz-1)+1:Lx*Ly*Lz,i) = 0;
    if i <= t_stim
        dVmdt(:,i) = mv(:,i)/(beta*Cm)+Istim/((beta*Cm)/1000)-Iion*2e-2/Cm;
%                 dVmdt(:,i) = (Istim)/((beta*Cm)/1000)-Iion*2e-2/Cm;
    else
        dVmdt(:,i) = mv(:,i)/(beta*Cm)-Iion*2e-2/Cm;
%                 dVmdt(:,i) = (0)/(beta*Cm)-Iion*2e-2/Cm;
    end
    %     dVmdt(1:Lx*Ly,i) = 0;
    %     dVmdt(Lx*Ly*(Lz-1):Lx*Ly*Lz,i) = 0;
    %     for kz = 2:Lz-1
    %         dVmdt((kz-1)*Lx*Ly+1:(kz-1)*Lx*Ly+Lx+1,i) = 0;
    %         dVmdt((kz-1)*Lx*Ly+(Ly-1)*Lx:(kz-1)*Lx*Ly+Lx*Ly,i) = 0;
    %         for ky = 2:Ly-2
    %             dVmdt((kz-1)*Lx*Ly+ky*Lx:(kz-1)*Lx*Ly+ky*Lx+1,i) = 0;
    %         end
    %     end
    for kz = 1:Lz
        dVmdt((kz-1)*Lx*Ly+1:(kz-1)*Lx*Ly+Lx+1,i) = 0;
        dVmdt((kz-1)*Lx*Ly+(Ly-1)*Lx:(kz-1)*Lx*Ly+Lx*Ly,i) = 0;
        for ky = 2:Ly-2
            dVmdt((kz-1)*Lx*Ly+ky*Lx:(kz-1)*Lx*Ly+ky*Lx+1,i) = 0;
        end
    end
    dVmdt(1:Lx*Ly,i)=0;
    dVmdt(Lx*Ly*(Lz-1)+1:Lx*Ly*Lz,i) = 0;

    Vm(:,i+1) = Vm(:,i)+dVmdt(:,i)*(delta_t/1000);
    disp(i);
end
```